Ghezzi *et al. Cell Communication and Signaling* (2025) 23:348
https://doi.org/10.1186/s12964-025-02361-2

Cell Communication and Signaling

RESEARCH Open Access

NAMPT and NNMT released via extracellular vesicles and as soluble mediators are distinguished traits of BRAF inhibitor resistance of melanoma cells impacting on the tumor microenvironment

Beatrice Ghezzi[1†], Irene Fiorilla[1†], Ágata Carreira[2,7†], Francesco Recco[1,3], Leonardo Sorci[4], Lidia Avalle[1], Alessia Ponzano[1], Francesca Mazzola[5], Alberto Maria Todesco[1], Nicoletta Tommasi[1], Massimiliano Gasparrini[6], Vito Giuseppe D'Agostino[2], Flavio Mignone[3], Alessandro Provenzani[2] and Valentina Audrito[1*]

Abstract

Drugs targeting mutant BRAF and MEK oncogenes are effective in melanoma, even though resistance rapidly develops. This complex picture includes acquired intrinsic tumor and tumor microenvironmental-mediated mechanisms. Here we show that melanoma cells resistant to BRAF inhibitors (BRAFi) overexpress the rate-limiting enzymes involved in nicotinamide (NAM) metabolism nicotinamide phosphoribosyltransferase (NAMPT) and nicotinamide N-methyltransferase (NNMT). Remarkably, these cells release NAMPT and NNMT both in the free-form or loaded into extracellular vesicles (EVs). NAMPT is emerging as a key mediator of resistance to BRAFi in melanoma, primarily due to its established role in NAD biosynthesis. Although previously identified as a soluble extracellular factor in this tumor, its presence within EVs released by melanoma cells has not been reported until now, highlighting a previously unrecognized mechanism through which NAMPT may influence the tumor microenvironment (TME). NNMT was revealed to increase in melanoma lesions compared to benign nevi. Here, we report for the first time its overexpression in resistant melanoma cell lines at intracellular and extracellular levels (secreted both as a soluble factor and into EVs). NNMT expression is increased in BRAF-mutated melanoma patients, suggesting a link between its upregulation and the BRAF oncogenic signaling. Moreover, NNMT levels positively correlate with gene signatures associated with pro-inflammatory signaling, immune cell migration, and chemokine-mediated pathways. NNMT pharmacological inhibition and genetic silencing significantly reduce resistant melanoma cell growth. In addition, we found that BRAFi-resistant cells are more sensitive to NNMT inhibition, highlighting a trait of vulnerability of BRAFi-resistant melanomas. Lastly, we proposed for the first time

†Beatrice Ghezzi, Irene Fiorilla, and Ágata Carreira contributed equally to this work.

*Correspondence:
Valentina Audrito
valentina.audrito@uniupo.it

Full list of author information is available at the end of the article

a tetrameric NNMT:TLR4 binding model offering a plausible structural and mechanistic basis for their association. Our functional results indicated that exogenous NNMT treatment is able to trigger NF-κB pathway, one of the main TLR4-dependent signaling, sharing this cytokine-like properties with NAMPT, and opening a future deeper exploration of its functional role in the extracellular space. Overall, the identification of NAMPT and, surprisingly also NNMT, included in EVs and abundantly released from resistant melanoma cells supports the impact of these moonlighting proteins involved in nicotinamide metabolism as mediators of BRAF/MEK inhibitors resistance with tumor intrinsic and potentially tumor microenvironment-mediated mechanisms. Interfering with nicotinamide metabolism could be a valid strategy to counteract drug resistance acting on the multifactorial tumor-host interactions.

Keywords NAMPT, NNMT, Metastatic melanoma, Resistance, Extracellular vesicles, Secretome, Signaling, Tumor microenvironment

Introduction

Tumors are characterized by a complex microenvironment composed of immune, stromal, and cancer cells [1, 2]. Soluble mediators released within this tumor microenvironment (TME) can promote tumor growth and therapy resistance [3]. This concept also emerged in metastatic melanoma (MM), where increasing evidence has demonstrated that extracellular proteins secreted by tumor cells (secretome) [4, 5], as well as proteins carried in the extracellular vesicles (EVs) originating from MM cells, shape the TME and drive the expansion of drug-resistant cells [6]. Therefore, in addition to resistance mechanisms relying on metabolic, epigenetic and gene expression reprogramming [7–12], it is emerging that an altered secretome and the molecular cargo of EVs contribute to acquired resistance to both BRAF/MEK targeted therapy [4, 13], effective in BRAFV600E-mutant MM patients (about 50% of MM patients), and immune checkpoint inhibitors (ICIs; anti PD-1/PD-L1 or CTLA-4 antibodies) [14].

Nicotinamide adenine dinucleotide (NAD) biosynthesis is essential to support tumor energetic needs, and to regulate the NADPH-mediated detoxification system [15, 16]. Moreover, it provides NAD to various NAD-consuming enzymes, including sirtuins and poly-ADP-ribose-polymerases (PARPs), activating epigenetic circuits and regulating DNA repair [15, 16]. To support NAD synthesis, required for metabolic adaptation mechanisms, proliferation, and invasion, several types of cancer show up-regulation of nicotinamide phosphoribosyltransferase (NAMPT), the rate-limiting enzyme controlling NAD biosynthesis from nicotinamide (NAM) [17–19]. For these reasons, patients bearing tumors addicted to NAMPT activity benefit from the NAMPT-targeting strategy [18, 20–22]. In MM, we and others previously demonstrated that NAMPT is overexpressed during BRAFi resistance and patient relapse/progression, becoming a driver of targeted-therapy resistance, modulating metabolic reprogramming [23–27]. Moreover, BRAFi-resistant MM cells are uniquely sensitive to NAMPTi in vitro and in vivo [23, 24], supporting a molecular connection between NAMPT and BRAF oncogenic pathways [23, 28].

The amount of NAM inside the cell, available for energy metabolism, can be regulated by a second emerging enzyme, i.e., the nicotinamide N-methyltransferase (NNMT) [29–35]. NNMT catalyzes the N-methylation of NAM using S-adenosyl-L-methionine (SAM) as the donor of the methyl group to generate 1-methylnicotinamide (MNA) and release S-adenosyl-L-homocysteine (SAH). The deregulation of NNMT levels and activity has been observed in various tumor types, promoting tumor development and progression and directly and indirectly impacting gene expression by influencing the SAM/SAH ratio inside the cell [29, 35–37]. However, a clear functional role of this enzyme in tumor biology should be investigated more deeply, as well as the interplay between NAMPT and NNMT in regulating nicotinamide metabolism and NAD availability in cancer cells.

NNMT was previously detected in skin cancer [38]. Ganzetti et al., first showed significantly higher NNMT expression in melanoma compared with benign nevi [39]. In addition, a significant inverse relationship was found between the enzyme levels and Breslow thickness, Clark level, the presence/number of mitoses, and ulceration. They suggested that NNMT could represent a molecular biomarker for melanoma, thus highlighting its potential for both diagnosis and prognosis of this neoplasia [39]. High NNMT levels were also detected in aggressive oral malignant melanoma (OMM), where univariate analysis showed a negative effect of NNMT expression on the disease-free survival rate [40]. Interestingly, NNMT was also highly expressed in metastatic lymph nodes compared to both primary melanomas and nevi [41]. The mentioned papers confirmed the overexpression of NNMT in melanoma, also highlighting the impact of NNMT inhibition or silencing in decreasing melanoma cells' proliferation and migration, as well as increasing cell sensitivity to chemotherapeutics, such as dacarbazine, leading to the hypothesis that NNMT might be involved in promoting mechanisms of chemoresistance [42]. However, the

function of NNMT was never linked with targeted-therapy resistance in MM.

Intriguingly, various enzymes involved in NAD metabolism are considered moonlighting proteins, exhibiting multiple functions depending on their localization in different cellular compartments or their role as soluble factors. This is the case of NAMPT that can be secreted in the extracellular space, where it behaves as a mediator of inflammation, like danger-associated molecular patterns (DAMPs), through binding to cell membrane receptors, including toll-like receptor 4 (TLR4) [43–45]. Extracellular (e)NAMPT levels, increased in many tumors, regulate tumor-host interactions. Once secreted, eNAMPT can act as a cytokine-like protein that modulates the immune response, triggering intracellular signaling that promotes differentiation/polarization of myeloid cells, activation of inflammasome, and secretion of pro or anti-inflammatory cytokines [18, 19, 44]. Circulating NNMT was found to be increased compared with healthy donors in non-small cell lung cancer and colorectal cancer, and in exosomes of gastric cancer patients [46–48], highlighting the potential function of eNNMT in the tumor microenvironment (TME), yet systematically unexplored. In addition, NAM and MNA metabolites are emerging as factors that can shape immune cells [49–51].

The aim of this work is to characterize the proteins differentially enriched in EVs and in the secretome of BRAFi-resistant melanoma cells compared to the sensitive ones. In this study, we show that NAM-metabolic enzymes NAMPT and NNMT were indeed highly deregulated, with increased abundancy in EVs and in culture media derived from resistant melanoma cell lines. Focusing on NNMT, we identified this enzyme as a pivotal protein increased as an intracellular and extracellular factor upon drug-resistance acquisition and correlated with the BRAF mutational status of MM patients. NNMT pharmacological inhibition and genetic silencing significantly reduced resistant melanoma cell growth. In addition, we found that resistant cells are more sensitive to NNMT inhibition, indicating an unraveled role of this enzyme in BRAF inhibitor resistance. Through bioinformatic analysis on the melanoma cohort from The Cancer Genome Atlas (TCGA), we found that NNMT expression positively correlates with pro-inflammatory signaling, immune cell migration, and chemokine-mediated signaling pathways. Moreover, based on our predictive modeling and functional validation, NNMT—when acting as a soluble protein—represents a potential novel ligand for TLR4, the same receptor recognized by NAMPT, and is able to trigger NF-κB signaling. These findings pave the way for future investigations into the potential role of eNNMT in TME remodeling, acting on both tumor and immune cells.

Materials and methods

TCGA and CCLE analysis

Genomic data shown in this paper are in whole or part based upon data generated by The *Cancer Genome Atlas (TCGA)* Research Network and The *Cancer Cell Line Encyclopedia (CCLE*).

The association between *NAMPT* and *NNMT* expression was evaluated using gene expression data for cutaneous melanoma cohort of patients (*TCGA-SKCM*) and melanoma cell lines selected from a CCLE dataset based on clinical annotations (In particular, cell lines with primary_disease "Skin Cancer" and Subtype containing the term "Melanoma" were considered). For TCGA data, normalized RNA-Seq data (*DESeq2*), transformed into *log2(normalized counts + 1)* were plotted for *NAMPT* and *NNMT* genes. Both the non-parametric Spearman correlation and the Pearson test were applied to the entire cohort. Statistical significance was assessed using *cor.test*, and results were visualized with scatter plots including a linear regression line (*ggplot2*), reporting the Spearman's rho coefficient, Pearson's r coefficient, and corresponding *p-values*. For CCLE dataset expression data for *NAMPT* and *NNMT* were extracted, and both parametric (Pearson) and nonparametric (Spearman) correlation analyses were performed for NAMPT-NNMT pair. The results were represented by a scatter plot with a linear regression line. The coefficient (R) and associated p-value were reported for each correlation.

NNMT association with BRAF mutations

Somatic mutations in the *BRAF* gene were extracted from *TCGA-SKCM Masked Somatic Mutation (MAF)* files, including all annotated variants (missense, synonymous, nonsense) without filtering for functional impact. Patients were classified as "Mutated" if at least one *BRAF* mutation was detected in any sample (primary or metastatic).

NNMT expression (*log2(normalized counts + 1)*) was compared between *BRAF*-mutated and wild-type groups using the non-parametric Wilcoxon test. Data distributions were visualized using violin plots generated with *ggplot2*, reporting the *p-value* for statistical significance.

Gene set enrichment analysis (GSEA)

RNA-Seq gene expression data for cutaneous melanoma (*TCGA-SKCM*) were retrieved using the *TCGAbiolinks* package, selecting samples classified as "Primary Tumor" and "Metastatic." Raw data were preprocessed by filtering out low-expression genes (*counts* > 1 in at least 20% of the samples) and normalized using the *median of ratios* method in *DESeq2*. Samples were then stratified into two groups (*NNMT_high* and *NNMT_low*) based on the median *NNMT* expression.

Differential expression analysis was performed using *DESeq2* with the design ~ NNMT_group. Genes with an FDR-adjusted *p-value* < 0.05 were used for Gene Set Enrichment Analysis (GSEA), focusing on biological processes from *Gene Ontology* (*GO*). The analysis was conducted using *clusterProfiler*, filtering for *FDR* < *0.05* and selecting terms related to selected categories as shown in the results. Results were visualized using *enrichplot* and *ggplot2*.

Cell culture

M14, A375 an SK-MEL-28 BRAFV600E-mutated melanoma cell lines were cultured in RPMI-1640 (Corning Inc., Cat #10-040-CV, Corning, NY, USA) and DMEM (Corning Inc., 10-013-CV) supplemented with 10% (v/v) fetal bovine serum (FBS, Capricorn Scientific, FBS-11 A, #CP21-4466, Ebsdorfergrund, Germany), 1% MEM Non-Essential Amino Acids Solution (Gibco, Thermo Fisher Scientific, #11140035, Segrate, MI, Italy), 1% MEM Vitamin Solution (Gibco, #11120037), 10 mM HEPES Buffer Solution (Capricorn scientific, HEP-B, #CP24-7334), Sodium pyruvate solution 100 mM (Capricorn scientific, NPY-B, #CP23-6474) and 1% Gentamycin (Gibco, #15750-037). Cells were maintained in these culture conditions for all experiments except where specifically indicated. All cell lines were routinely tested for Mycoplasma contamination. During the generation of BRAFi resistance as described in [23, 52], parental cell lines were exposed to increased concentrations of the (Dabrafenib or Vemurafenib). Cells were considered fully resistant when they could grow in the presence of 1.6 μM of BRAFi.

THP-1 cell line was provided by Prof. Nadia Raffaelli (Polytechnic University of Marche, Ancona, Italy), and cultured in RPMI-1640 supplemented with 10% FBS, following the manufacturer's instructions.

RNA extraction and quantitative real-time PCR (qRT-PCR)

RNA was isolated from cells using NucleoSpin® RNA (Macherey-Nagel, #FC140955N, Düren, Germany) according to the manufacturer's instructions and quantified using kit/Qubit (Qubit™ RNA BR Assay Kits #Q10210, Thermo Fisher Scientific).

RNA was converted to cDNA using the High-Capacity cDNA Reverse Transcription kit (Thermo Fisher Scientific, 4368814). qRT-PCR was performed using the CFX384 (Bio-Rad Laboratories Srl, Segrate MI, Italy) Real-time System using commercially available primers [TaqMan Gene Expression Assays (Thermo Fisher Scientific): Hs00237184_m1 (*NAMPT*), Hs00196287_m1 (*NNMT*) and Hs99999903_m1 (*ACTB*, used as housekeeping gene)]. Comparative CT methods was used to calculate the relative expression of the gene under analysis [53].

Western blot analysis

Cells were lysed with cold lysis buffer (HEPES 20 mM, NaCl 150 mM; 1mM EGTA; phenylarsine oxide 50 μM) supplemented with 1 mM PMSF, 1 mM Na_3VO_4, 50 mM NaF, 1X complete Protease Inhibitors Cocktail (Sigma-Aldrich S.r.l., #P8340-5ML Milan, Italy), 10 mM iodoacetamide and 1% NP-40. Lysates were centrifuged at 14,000 g for 15 min at 4 °C, and protein concentration was measured using the Bradford assay (Bio-Rad, #5000006). Lysates were diluted in Laemmli buffer (Bio-Rad, #161–0747) and boiled for 5 min at 95 °C. Equal amounts of proteins were loaded on 4–20% Mini- PROTEAN® TGX™ Precast Protein Gels (Bio-Rad, #4568084) and transferred to Nitrocellulose Transfer Membrane (Trans-Blot Turbo RTA Midi 0.2 μm Nitrocellulose Transfer Kit, for 40 blots #1704271). Membranes were blocked in 5% non-fat dry milk (SERVA Electrophoresis GmbH, #42590.01, Heidelberg, Germany) in Tris-buffer saline, 0.1% Tween20 (ITW Reagents S.R.L., #A4974,0500, Monza, MB, Italy) and incubated with the indicated antibodies following the manufacturer's instructions. The following antibodies were used: NAMPT (Bethyl Laboratories, #A300-779 A, Montgomery, Texas, USA); NNMT #E6N22 and Phospho-NF-κB p65 (Ser536) #3033 (both from Cell Signaling Technology, Danvers, Massachusetts, USA; and OriGene Technologies, #TA502624, Rockville, MD, USA); TSG101 #GTX70255 and Vimentin #GTX100619 (both from GeneTex, Irvine, CA, USA); CD9 ab236630; Calnexin ab22595 and Syntenin ab133267 (all from Abcam, Cambridge, UK); β-Actin sc-47,778, TLR4 sc-293,072, Vinculin-HRP sc-73,614 and NF-κB-p65 sc-8008 (all from Santa Cruz Biotechnology, Dallas, Texas, USA).

Secondary Abs were mouse anti-rabbit IgG-HRP (Santa Cruz Biotechnology, sc-2357); Peroxidase AffiniPure goat Anti-Rabbit IgG (Jackson ImmunoResearch West Grove, Pennsylvania, USA, #111-035-003), mouse-IgGκ BP-HRP (Santa Cruz Biotechnology, sc-516102) and Peroxidase AffiniPure goat Anti-Mouse IgG (Jackson ImmunoResearch, 115-005-003).

Western blot chemioluminescence reactions were visualized with ECL (Clarity Western ECL Substrate, Bio-Rad, #170–5060) using iBright™ CL1500 Imaging System (Thermo Fisher Scientific) or the ChemiDoc XRS imaging systems (Bio-Rad). Densitometric analyses performed using Bio-Rad Image lab software 6.1 version and iBright Analysis Software V5.3.0. Total proteins were normalized over actin or calnexin levels.

Confocal microscopy

A375 and M14 (S and BiR) cell lines were seeded in a 96-well cell carrier plate (PerkinElmer), and fixed and permeabilized the day after with 4% paraformaldehyde (PFA) for 12 min, and 0.1% Triton X-100 in PBS for

10 min, respectively, always at room temperature. Following incubation with blocking solution (3% BSA in PBS) for 30 min, cells were incubated with the primary antibodies for 2 h. The primary antibodies used were: Anti-NNMT (OriGene, #TA502624, 1:250) and Goat Anti-Mouse AF467 (Invitrogen, Thermo Fisher Scientific, #A-21235, 1:500).

Hoechst (Invitrogen, H1399; 1.5 µg/ml) in PBS + BSA 0.6% was used to detect nuclei. Fluorescence images were acquired using the PerkinElmer image plate reader Operetta and evaluated using the Harmony 3.5.2 software. For each well, images were acquired in seven preselected fields of view with a 10× objective over two channels: blue [fluorescence excitation (λEx), 377/54 nm; fluorescence emission (λEm), 432/36 nm] and far red (λEx, 635/22 nm; λEm, 692/40 nm). Three biological replicates were acquired.

Preparation of culture supernatants (SN) for eNNMT quantification and secretome analysis

2,5 million MM cells (M14, A375 and SKMEL-28 in S and BiR variant) were seeded in 10 cm culture dishes. After 48 h, cells were washed twice with PBS and incubated for additional 24 h with FBS-deprived medium. The collected media was centrifuged at 2,800 rcf for 15 min to eliminate cell debris and larger cellular-derived particles. The culture supernatant (SN) was then concentrated 10x using Amicon Ultra – 0.5 ml Centrifugal Filters cutoff 10 kDa (Ultracel, UFC501024, Merk Life Science S.r.l., Milan, Italy). The collected 50ul of 10x SN, resuspended in Laemmli buffer (Bio-Rad, #161–0747) and boiled for 5 min at 95 °C, was loaded in SDS-PAGE followed by western blot analysis to evaluate eNNMT (same Abs used for lysates). The intensity of the bands corresponding to eNNMT was normalized over the protein concentration (µg/µl) of specific samples.

The SNs (FBS free-media) for secretome MS-analysis were collected, centrifuged at 2000 × g at 4 °C for 10 min and filtered through a 0.2 µm filter to ensure the removal of any dead cells and then ultracentrifuged at 100,000 x g for 70 min at 4 °C to eliminate extracellular vesicles (EVs) and subsequent processed for proteomic analysis as described below.

In a set of experiments, we treated or not SNs from A375 and SK-MEL-28 BiR variants with 100 ng/ml of Proteinase K (ProK, EO0491, Thermo Fisher) for 1 h at 37 °C after ultracentrifugation (100,000 x g for 70 min at 4 °C) [54]. Collected SNs were concentrated 10X using Amicon Ultra – 0.5 ml Centrifugal Filters cutoff 10 kDa, as previously described. ProK digestion degrades the free-soluble proteins (Vimentin was used as positive control) while leaving almost unaffected the exosomes' integrity (Syntenin was used as exosome control).

Extracellular vesicles (EVs) isolation

For EVs isolation, 2,5 million of MM cells (M14 and A375 in S and BiR variant) were seeded in 10 cm culture dishes. After 48 h, cells were washed twice with PBS and incubated for additional 24 h with FBS-deprived medium. The collected media was centrifuged at 2,800 rcf for 15 min to eliminate cell debris and larger cellular-derived particles. The supernatant was ultracentrifuged at 100,000 rcf for 70 min at 4 °C in an Optima XE-90 ultracentrifuge with a SW 32 Ti rotor (Beckman Coulter). Finally, the supernatant was kept at -80 °C until further processing, while the EVs pellet was resuspended in 0.22 µm-filtered sterile PBS and stored at 4 °C.

EVs characterization and quantification

Particle size distribution and concentration were determined by nanoparticle tracking analysis (NTA) with NanoSight NS300 (Malvern Panalytical, Malvern, UK). Individual samples were recorded in 3–5 consecutive 1-minute videos at camera level 15, gain 1, and analyzed with NTA 3.4 Build 3.4.003 (Malvern Panalytical), setting 4 as a detection threshold. The quality of isolated particles was also assessed by western blot analysis using dedicated markers (see specific Abs used in the western blot analysis section).

Proteomics analysis

Sample Preparation

Isolated EVs were lysed in RIPA buffer for 30 min at 4°C. Samples were adjusted to a final concentration of 1% SDS, 50 mM HEPES, benzonase 250U/ml, and sonicated at 4°C for 10 min using a Q700 Sonicator (30" on and 30" off, amplitude 35).

For secretome analysis, the secreted proteins in the culture media were precipitated by well-established TCA-DOC method [55]. The washed pellets were air-dried and dissolved in 2% SDS, 100 mM HEPES.

The total protein content EV lysates and secretome samples was assessed using a BCA assay. Afterward, EVs and secretome samples (20 µg) were reduced using 10 mM dithiothreitol (DTT) for 30 min at 56 °C and alkylated for 30 min using 22.5 mM iodoacetamide (IAA) in the dark at room temperature. Protein digestion was performed using a 1:1 ratio of magnetic carboxylate-modified beads (GE Healthcare) as described before [56]. Briefly, washed beads were added to the samples in a ratio of 10 µg of beads to 1 µg of protein. Afterward, acetonitrile (ACN) was added to a final concentration of 70% (v/v), and samples were mixed at room temperature for 18 min. Supernatants were removed, and beads were washed twice with 70% ethanol and once with ACN (200 µl each). Beads were then resuspended in 45 µL of 50 mM NH4HCO3 and 5 mM CaCl2 supplemented with one µg of trypsin. After overnight digestion at 37 °C, the

peptide mixture was collected by incubation on a magnetic rack. The beads were then washed with 15 µl of NH4HCO3, and the supernatant was pooled with the previously collected. For peptide cleanup, samples were processed using SP2 method [57]. Peptide mixtures were bound to magnetic carboxylate-modified beads (GE Healthcare) in a ratio of 1:15 by the addition of one volume of acetonitrile and washed twice with 100% acetonitrile. After drying, elution was performed using 2% ACN in water. Peptides were then acidified at a final concentration of 0.1% (v/v) formic acid and stored at -20° C for further processing.

nLC-MS/MS analysis

An Easy-nLC 1200 HPLC system (Thermo Fisher Scientific) with a 30 cm long C18 column and integrated electrospray emitter (CoAnn Technologies, ID 75 µm, 1.7 µm, 100Å, Richland, Washington, USA), heated to 40 °C, was used for peptide separation at a flow rate of 200 nL/min. The separation was carried out with a two-component mobile phase system consisting of 0.1% formic acid in water (buffer A) and 0.1% formic acid in 80% acetonitrile (buffer B). Peptides were eluted using a gradient from 5 to 25% buffer B over 52 min, followed by 25–40% over 8 min, and 40–98% over 10 min.

The peptides were analyzed on an Orbitrap Fusion Tribrid mass spectrometer (Thermo Fisher Scientific) in data-dependent mode, with the full scans performed at a resolving power of 120.000 FWHM (2100 V, mass range: 350–1200 m/z, AGC target value: 1 × 10e6 ions, maximum injection time: 50 ms). Each full scan was followed by a set of (HCD) MS/MS scans within a 3 s cycle time, with a collision energy of 27%. Fragment data were acquired in the ion trap mass analyzer (AGC target: 5e4 ions, maximum injection time: 150 ms). The Ion transfer tube temperature was set at 200 °C. Dynamic exclusion was enabled and set to 40 s, with a mass tolerance of 5 ppm. Data were acquired using Xcalibur 4.3 and Tune 3.3 software (Thermo Fisher Scientific). QCloud [58] was used for all acquisitions to control long-term instrumental performance during the project, using quality control standards.

All proteomic data were searched against the in-silico digested UniProt *Homo sapiens* (downloaded in January 2024) with major known contaminants and reversed versions of each sequence. Proteome Discoverer v.2.2.0 (Thermo Fisher Scientific) and MASCOT search engine (v.2.6.2, MatrixScience, London, UK) were used to identify proteins (precursor mass tolerance: 10 ppm, product mass tolerance: 0.6 Da). Trypsin/P was chosen as the enzyme with 5 missed cleavages. Static modification of carbamidomethyl (C) and variable modification of oxidation (M) and N-terminal protein acetylation were incorporated in the search. FDR was set to < 0.01 for both peptides and proteins. Contaminants were filtered out.

MS computational analyses

MS downstream analysis was performed using the ProTN proteomics pipeline (www.github.com/TebaldiLab/ProTN and www.rdds.it/ProTN). In summary, peptide intensities were log2 transformed, normalized (median normalization), and summarized into proteins (median sweeping) with functions in the DEqMS Bioconductor package [59]. Imputation of the missing intensities was executed by the PhosR package [60]. Differential analysis was performed with the DEqMS package, proteins with absolute log2 FC > 0.75 and P-value < 0.05 were considered significant. Functional enrichment analysis of differentially expressed proteins was performed with ClusterProfiler function EnrichGO and using Enrichr https://maayanlab.cloud/Enrichr/ and https://appyters.maayanlab.cloud/Enrichment_Analysis_Visualizer [61]. Enriched terms with p-value lower than 0.05 were considered significant.

MS data availability

The mass spectrometry proteomics data have been deposited to the ProteomeXchange Consortium via the PRIDE [62] partner repository with the dataset identifier PXD063060 and https://doi.org/10.6019/PXD063060.

Cell transfection and lentivirus infection

Specific siRNA for NNMT (siNNMT, sc-61213) and negative control siRNA (siCTR, siRNA-A: sc-37007) both from Santa Cruz Biotechnology) were transfected (0.02 µg/transfection) in 96-w plate using Lipofectamine 2000 Transfection Reagent (Invitrogen, USA), according to the manufacturer's protocol. After 48–72 h of transfection, the cells were harvested for subsequent experiments. Silencing efficacy was tested by RT-PCR analysis.

For NNMT knockdown experiments, the shNNMT RNA cassette (Target sequence: 5' GCTCAAGAGCA GCTACTACAT 3') was cloned into the pLKO plasmid (Addgene, Plasmid #10879). The PLKO shNNMT plasmid was amplified and sequence was confirmed through Sanger sequencing. Lentiviral particles were produced by EffeCtene (QIAGEN, cat. 301425) as described in http://tronolab.epfl.ch/. Viral supernatants were collected and filtrated 72 h post-transfection. Puromycin selection (2 µg/mL) was performed for 3 days before starting the experiments. pLKO empty vector was used as control. Silencing efficacy was tested by western blot analysis.

Cell proliferation assay

Cell viability was determined using Cell Counting Kit-8 (96992-500TESTS-F, Sigma-Aldrich, Merck KGaA, Darmstadt, Germany) according to the manufacturer's

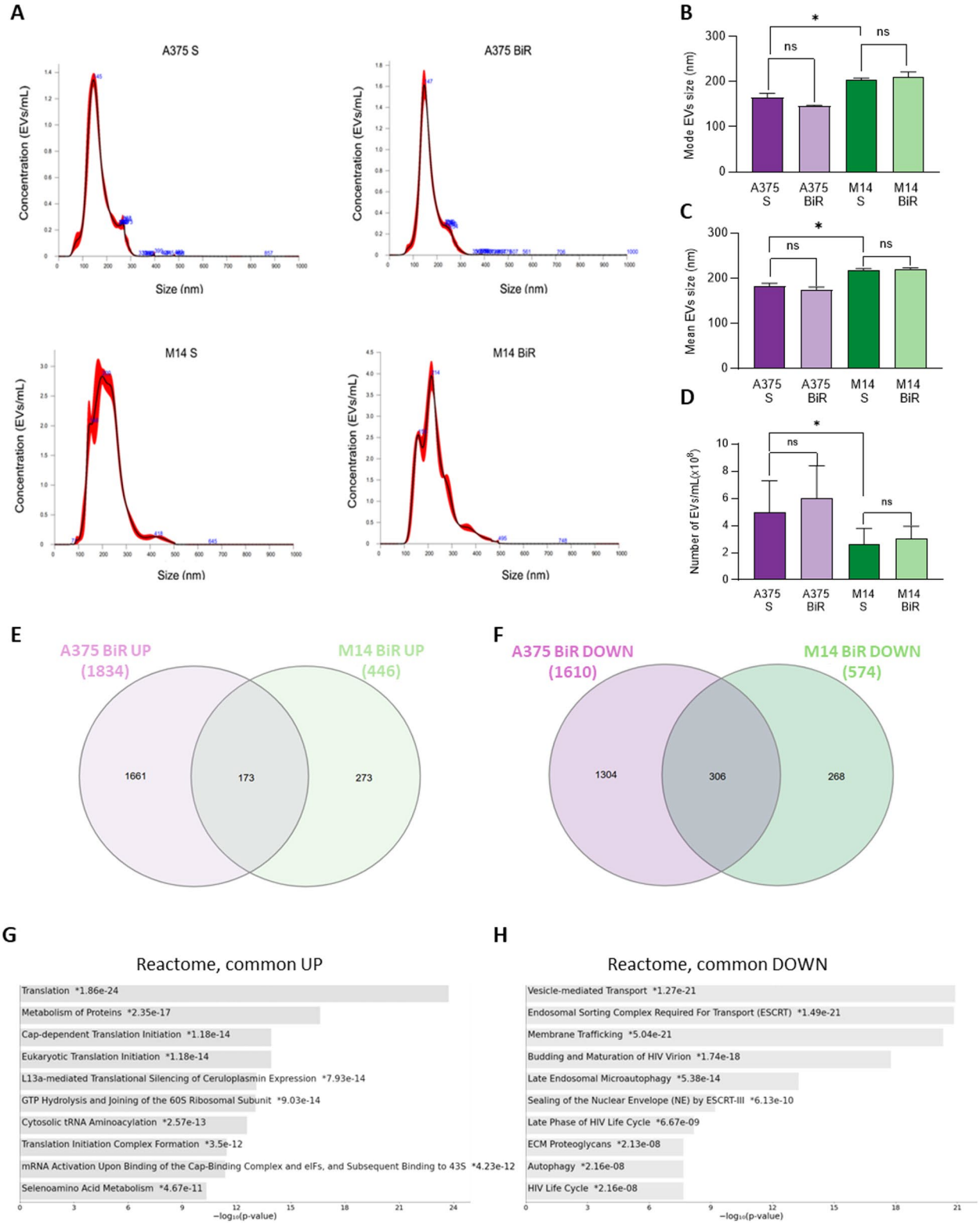

Fig. 1 (See legend on next page.)

(See figure on previous page.)

Fig. 1 Characterization of EVs isolated from melanoma cell lines. (**A**) Representative size distribution profiles from Nanoparticle Tracking Analysis (NTA) of EVs secreted from BRAF-mutated melanoma cell lines A375 and M14 sensitive (S) and BRAF-inhibitor resistant (BiR) are shown. The black curve represents the mean of three measurements, with standard error in red. (**B**) Mode, (**C**) mean EVs' diameters, along with (**D**) EVs number per mL, are plotted. Error bars represent at least three biological replicates. Repeated measures one-way ANOVA was used to calculate statistical significance (ns- not significant, *$p < 0.05$) between BiR and S cells. Venn diagrams indicating the number of proteins commonly (**E**) up and (**F**) downregulated in A375 and M14 BiR, identified by proteomics, and respectively reactome enrichment analysis of (**G**) up and (**H**) downregulated proteins. All the significant modulated proteins (p-value above 0.05) compared with the BRAF inhibitors sensitive A375 and M14 (A375 S; M14 S) cell lines were considered. Four independent biological replicates were considered for statistical analysis

instructions. To test the capacity of NNMT inhibitor (NNMTi, HY-131042, MedChemExpress, Sollentuna, Sweden) to block cell proliferation, we treated cells with the indicated concentrations (25-50-100 μM) for 72 h, as previously used in other tumor models [63, 64]. NAMPT inhibitor FK866 (S2799, Selleckchem, Munich, DE) 50 nM was used as positive control of cell growth arrest [23].

For the colony formation assay, 500 cells were plated into a six-well plate and maintained in culture media supplemented with 10% FBS for 10–12 days. At the same time, the medium with or without NNMTi was changed every three days. Then the clones were fixed with methanol, stained with 0.1% crystal violet and photographed. The percentage of occupied colony areas was calculated with ImageJ/Fiji software. All the experiments were repeated as indicated.

NNMT: TLR4 binding prediction

Structural models of the human NNMT: TLR4 heterotetramer were built using AlphaFold-Multimer v2.3.0 [65, 66], accessed through ColabFold [67]. The sequences of TLR4 (accession ID: O00206) and NNMT (accession ID: P40261) were taken from the UniProt database. Five predictions were obtained, one for each neural network model, and we selected the one with the highest combined predicted Template Model (pTM) and interface pTM score for Fig. 8C. All images were generated using Molsoft ICM 3.9-4 [68].

Signaling experiment using NNMT Recombinant protein

THP-1 monocytes are differentiated into macrophages by 48 h of incubation with 150 nM phorbol 12-myristate 13-acetate (PMA, HY-18739, MedChemExpress) in complete RPM1, and then recovered for 24 h in medium without serum. Differentiated THP-1 were treated for 30 min at 37 °C in medium without FCS with indicated doses (ng/ml) of recombinant human NNMT (Catalog # 7736MT, R&D System, Minneapolis, MN, USA) and, as positive control, with the same concentration of recombinant human NAMPT provided by Prof. Raffaelli's lab and previously characterized [45, 69]. In a set of experiments A375 BiR were starved for 24–30 h in medium without serum and then treated with the recombinant proteins as described for THP-1.

Cells were then lysed and p65 phosphorylation status, as a readout of NF-κB signaling activation, was analyzed by western blot.

Statistical analysis

Statistical analyses were performed using GraphPad Prism version 9.0 (GraphPad Software Inc., La Jolla, CA, USA). Statistical significance was assessed using an unpaired or paired Student's *t*-test, following a Shapiro-Wilk test to evaluate the normality of data distribution. One-way ANOVA was also used where indicated. Unless otherwise indicated, data in the Figures are presented as the mean ± SEM.

For all statistical tests, the 0.05 level of confidence was accepted for statistical significance. Significance was represented as: * $p \leq 0.05$, ** $p \leq 0.01$, *** $p \leq 0.001$, **** $p \leq 0.0001$.

Results

Proteomic characterization of EVs derived from BRAF inhibitor-resistant cells

The presence of eNAMPT in EVs was previously described in the context of ischemic injury, in mice to extend longevity, and in humans following moderate-intensity exercise [70–74]. Exosomal NAMPT was recently identified in leukemia with the effect of orchestrating monocyte survival [75], in aggressive brain tumor glioma as a mediator of radioresistance [76] and in colorectal cancer as biomarker [77]. To our knowledge, in melanoma, even if soluble eNAMPT was previously detected [26, 78], evidence of eNAMPT in EVs is missing. These observations provided an intriguing rationale to investigate the presence of eNAMPT in EVs in melanoma, with a special focus on molecular mechanisms behind melanoma resistance. Therefore, we conducted a proteomic analysis to compare EVs derived from BRAF inhibitor-sensitive (S) and -resistant (BiR) melanoma cells. This approach aimed to assess global proteomic alterations in EVs from resistant cells and to specifically investigate whether NAMPT is selected as EV cargo, potentially representing a mechanism for sharing active metabolic enzymes between tumor, inflammatory, and immune cells. Culture supernatants from two different BRAF-mutated melanoma cell lines, previously characterized [23, 52, 79] were collected, and EVs were isolated by differential ultracentrifugation. Representative

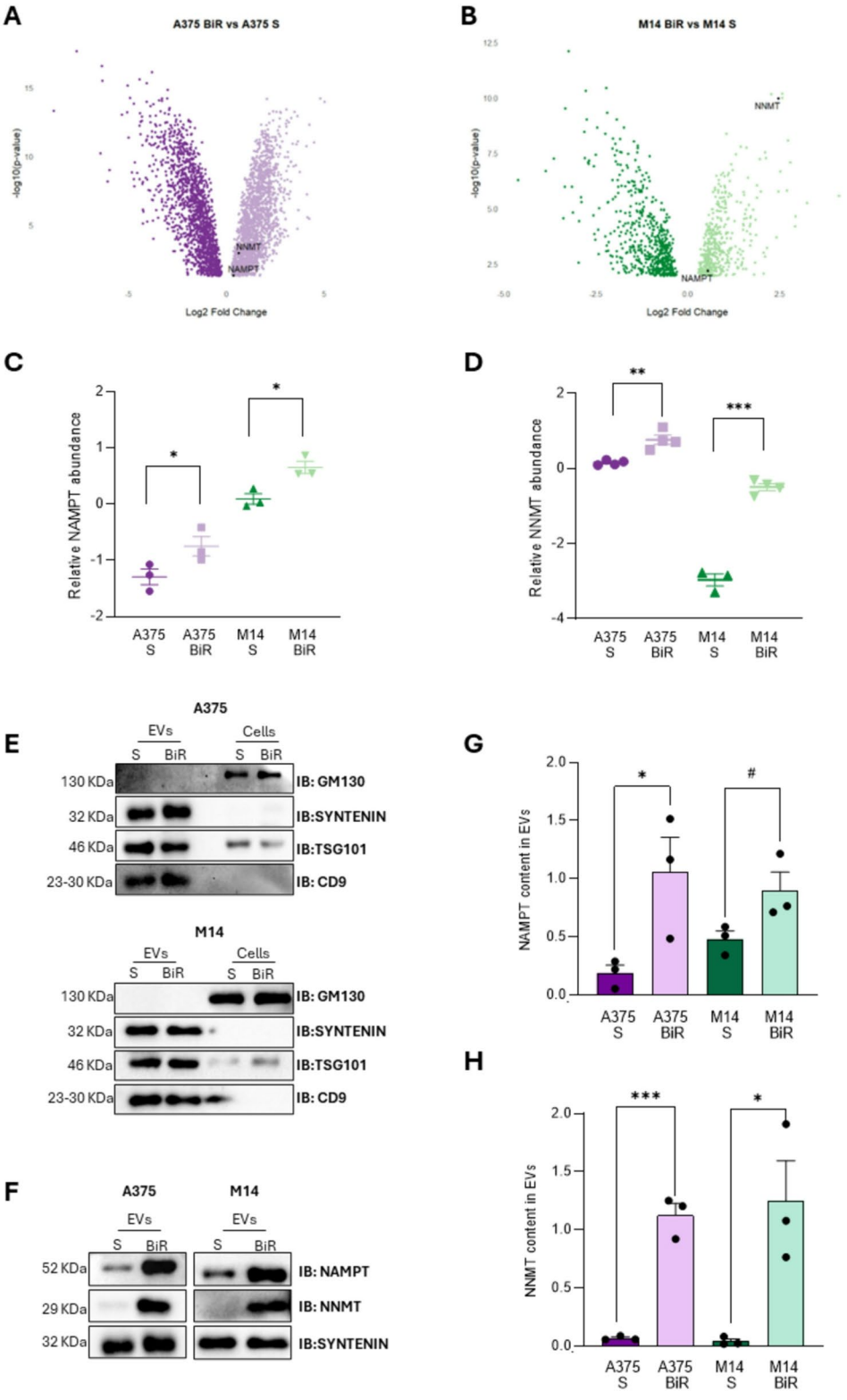

Fig. 2 (See legend on next page.)

(See figure on previous page.)

Fig. 2 NAMPT and NNMT are enriched in EVs from BiR cells. Volcano plots of significantly modulated proteins in (**A**) A375 BiR and (**B**) M14 BiR cell lines, compared with their respective sensitive counterparts (A375 S and M14 S). Black dots with labels for NAMPT and NNMT in each comparison are shown. Proteomics quantification of (**C**) NAMPT and (**D**) NNMT relative abundance in EVs isolated from the different cell lines. Repeated measures one-way ANOVA was used to calculate statistical significance (*$p < 0.05$, **$p < 0.01$, ***$p < 0.001$) between BiR and S cells. (**E**) Representative western blot images of EVs positive (TSG101, Syntenin, CD9) and negative (GM130) markers, as well as (**F**) NAMPT and NNMT expression in EVs isolated from A375 S, A375 BiR, M14 S and M14 BiR cell lines, and the respective cell lysates. Histograms reporting (**G**) NAMPT and (**H**) NNMT relative quantification in EVs, using syntenin as loading control to normalize data [80]. Three independent biological replicates were performed. Unpaired t-test was used to calculate statistical significance (*$p < 0.05$, **$p < 0.01$, $^{\#}p = 0.07$) between BiR and S cells in each cell line

nanoparticle tracking analysis (NTA) profiles of particles recovered from individual conditions are shown (Fig. 1A) and revealed that EVs mode (Fig. 1B) and mean size (Fig. 1C) as well as the number of released EVs (Fig. 1D) were comparable between S and BiR for both melanoma cell lines. Interestingly, A375 S cells secrete a smaller but slightly higher number of particles than M14 S (Fig. 1B-D). Immunoblotting of these particles, as shown in Fig. 2E, confirmed the presence of Syntenin, TSG101 and CD9 EV markers, expected with the ultracentrifugation protocol applied [80].

To characterize the protein cargo of recovered particles, we performed a proteomic analysis which revealed 1834 proteins significantly upregulated (p-value < 0.05) in A375 BiR compared to A375 S, and 1610 proteins downregulated in the same condition (Supplementary Material 1). Instead, 446 and 574 proteins were found respectively up- and down-regulated in M14 BiR compared with M14 S (Supplementary Material 1).

To investigate a common EVs signature in resistant MM cells we examined whether certain proteins were commonly modulated in EVs derived from both A375 and M14 BiR cell lines compared with the respective counterparts (S cells). We found 173 and 306 proteins, respectively up and down-regulated in BiR cells as shown in Venn diagrams (p-value < 0.05, Fig. 1E-F, Supplementary Material 2), which were independently subjected to gene set enrichment analysis. The gene ratio was determined by the number of modulated terms in each condition, that were part of a particular gene set, divided by the total number of terms annotated for that gene set. Through functional annotation databases such as gene ontology (GO), KEGG and Reactome, we observed an upregulation of terms associated mainly with protein translational processes and metabolism, in BiR cells (Fig. 1G, Supplementary Fig. 1A). Instead, downregulated terms point out a significant downregulation of endosomal transport pathway and ESCRT-dependent vesicular trafficking (Fig. 1H, Supplementary Fig. 1B). In line with the non-significant differences in the relative abundance of particles released by these cells, this observation indicates that resistant cells secrete a dramatically deranged EV quality.

Interestingly, the GSEA of proteins specifically up-regulated in EVs derived from the A375 BiR cells compared with their sensitive counterparts, additionally revealed an upregulation of the citrate cycle (Supplementary Fig. 2A-B), in line with the observed increased mitochondrial activity of these cells [23, 52]. Instead, particles from M14 BiR samples presented an upregulation of proteins involved in several metabolic processes, such as purine, ribonucleotide and aminoacid metabolism (Supplementary Fig. 3A-B). Downregulated terms are similar in the two cell lines, mainly involving cytoskeleton organization and endocytosis (Supplementary Figs. 2 and 3 panels B).

Overall, these data revealed that the acquisition of resistance to BRAF inhibitors does not influence EVs diameter or number, but is rather cell-line specific, with M14 releasing fewer but slightly larger EVs than A375 cells. The EVs cargo, instead, revealed that BiR-derived EVs are enriched in terms associated with translational processes, along with distinct metabolic signatures unique to each cell line, but mirroring common pathways activated/deactivated in BRAFi resistance.

NAMPT, but also NNMT proteins are enriched into EVs released from BiR cells

A closer analysis of the proteomics results revealed a significant enrichment of NAMPT in BiR cells-derived EVs (both in A375 and M14), reflecting its increased intracellular expression [23](Fig. 2A-C). The presence of NAMPT suggests an alternative mechanism of NAMPT exchange within the TME between tumor cells as well as between tumor cells and between tumor and immune cells. Surprisingly, a second enzyme, NNMT, involved in the catabolism of nicotinamide (i.e., methylation of nicotinamide) was concomitantly found in EVs from both BiR cell lines (Fig. 2A-B, D, Supplementary Material 2). NNMT transfer via EVs could represent an intriguing and novel hallmark in cancer cell communication. Interestingly, we revealed additional common up-regulated proteins in EVs, from both BiR cell variants. Nucleophosmin 1 (NPM1), which is associated with immune evasion and tumor progression [81], forces the expression of PD-L1 [82]. Proteins involved in stress granule (SGs) assembly [83], including ATXN2L, OGFOD1, FMR1, PRRC2C, EIF2S1, and PUM2 were highlighted. SGs emerged as regulators of the tumor immune microenvironment, leading to immune escape in tumor cells [84]. Interferon-gamma inducible protein 16 (IFI16), a DNA sensor protein, which triggers interferon-beta (IFN-β) production and inflammasome complex and IL-1β production [85],

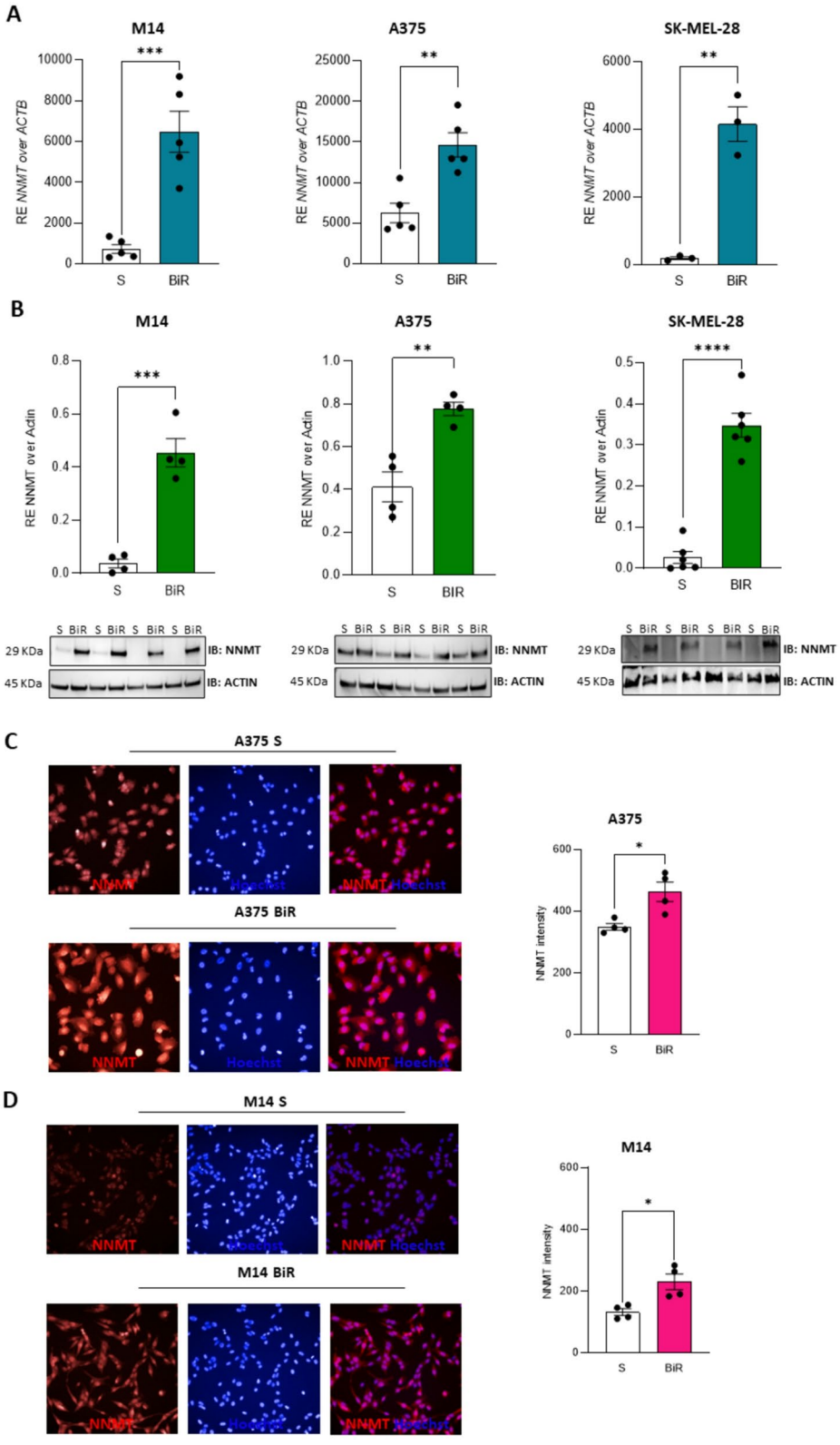

Fig. 3 (See legend on next page.)

(See figure on previous page.)

Fig. 3 NNMT is overexpressed in BiR cell lines. (**A**) Histograms reporting *NNMT* mRNA expression levels in S and BiR MM cell lines (M14, A375 and SK-MEL-28). Data from five independent experiments. (**B**) Analysis of NNMT expression in the same cell line variants by immunoblot. Actin was used as a loading control. Histograms show cumulative data of band quantification (at least $n = 4$) represented as a ratio of the enzyme/actin levels. Below the graphs are reported representative western blots. (**C**) NNMT expression evaluated by confocal immunofluorescence staining. Representative images of immunostaining of NNMT (red fluorescence) in (**C -** left) A375 S and BiR and (**D-**left) M14 S and BiR cell lines. Hoechst was used to stain the nuclei. Images were acquired with the Operetta instrument and Harmony 3.5.2 software. NNMT mean signal intensity in (**C**-right) A375 and (**D-**right) M14 cell lines was calculated with Harmony software. Statistical significance was calculated using unpaired t-test. Data in the graphs are presented as the mean ± SEM. Significance was represented as: $^{**}p \le 0.01$, $^{***}p \le 0.001$, $^{****}p \le 0.0001$

has recently been linked with M1-macrophage infiltration in melanoma [86]. Lastly, we found enriched in EVs also signal transducer and activator of transcription 3 (STAT3), linked with TLR4 signaling in melanoma [87], and DNA methyltransferase 1 (DNMT1) [88]. Notably, EVs isolated from A375 BiR cells exhibit strong upregulation of CD274/PD-L1, a key molecule involved in immune escape [89] and associated with shorter overall survival in melanoma [90]. PD-L1 expression, increased in BRAFi-resistant melanoma [79], was recently associated with the NAD/NAMPT axis [91, 92].

To validate the proteomics data, we performed an immunoblot with independent EV isolated from both S and BiR A375 and M14 cell lines. Importantly, the EVs positive markers Syntenin, TSG101 and CD9 were enriched in the EVs fractions but not in the respective cell lysates, differently from the Golgi marker GM130, which is not sorted into EVs (Fig. 2E). We confirmed the up-regulation of both NAMPT and NNMT in EVs isolated from BiR cells (Fig. 2F-H).

NNMT is upregulated in cell extract from resistant melanoma cells

NAMPT was previously reported to be overexpressed in resistant cells, acting as the master regulator of NAD synthesis and playing a key role in metabolic reprogramming during the acquisition of BRAFi resistance in melanoma [23, 24, 52]. NNMT results overexpressed in melanoma compared to benign nevi [38]; however, it was never associated with BRAFi resistance. Therefore, we focused on this enzyme to compare its intracellular and extracellular expression in BRAF-mutated melanoma cell lines sensitive and resistant to BRAFi. We found that *NNMT* gene was significantly upregulated in three different BiR cell lines (M14, A375, and SK-MEL-28; Fig. 3A). Parental (sensitive) M14 and SK-MEL-28 expressed low basal levels of *NNMT* compared to A375, strongly induced in BiR cell variants. Moving to the NNMT protein expression, immunoblot (for all BiR lines, Fig. 3B) and confocal microscopy (for A375, Fig. 3C and M14, Fig. 3D) analyses confirmed selective and robust upregulation of NNMT in BiR cells. Overall, this evidence demonstrated for the first time that, as for NAMPT, also NNMT is overexpressed at mRNA and protein levels in resistant cells, opening future studies investigating its role in the onset of BRAFi resistance and corresponding TME.

eNNMT is released as a soluble protein by melanoma cells, increasing in resistant cells

We detected NAMPT and NNMT in EVs, increasing in BiR cells. eNAMPT is an established soluble factor released as free protein from different cellular models, especially in inflammatory and metabolic conditions, and in tumors [44, 93]. Melanoma cell lines and patients release eNAMPT, becoming a novel marker of tumor burden [26, 78]. Circulating NNMT was identified in NSCLC and colon cancer [46, 48]. For the first time, we revealed the presence of eNNMT by western blot, analyzing 10x concentrated conditioned media without serum for 24 h from the same 3 representative BRAF-mutated melanoma cell lines S vs. BiR (Fig. 4A-C). eNNMT detected in western blot could be secreted either in EVs or as a free protein in the supernatant. The quantification of the relative proportion of free *versus* EV-containing protein is a difficult task that we tried to address experimentally. We ultracentrifuged supernatants from A375 and SK-MEL28 BiR variants and then treated or not with Proteinase K (ProK, 100 ng/ml, 1 h at 37 °C) [54]. Supernatants were concentrated 10X and loaded into the gel. ProK digestion is expected to degrade free-soluble proteins (vimentin used as positive control) while leaving almost unaffected the vesicles' integrity (assessment of syntenin levels as EVs marker). As reported in Fig. 4D-E, ProK digestion completely degraded Vimentin. Syntenin levels were unaffected by the treatment in SK-MEL-28 BiR, while partially reduced in A375 BiR, suggesting cell-dependent differences. eNNMT showed the same behavior: it was partially reduced after ProK treatment in both cell line SNs, suggesting at least the experimentally detectable dual secretion paths.

Overall, our data revealed the presence of soluble eNNMT released by melanoma cells, increased in BRAFi-resistant cells derived either from exosomes and released as a free protein.

eNNMT was confirmed highly enriched in the secretome of BiR cells

To confirm that the protein detected in culture supernatants (SN) was indeed NNMT, we used MS, selecting the A375 cell line (higher levels of eNNMT detected, Fig. 4B) to obtain and compare all the proteins "secretome" from SN derived from A375 S and BiR (4 biological replicates). Proteomics analysis revealed a significant upregulation

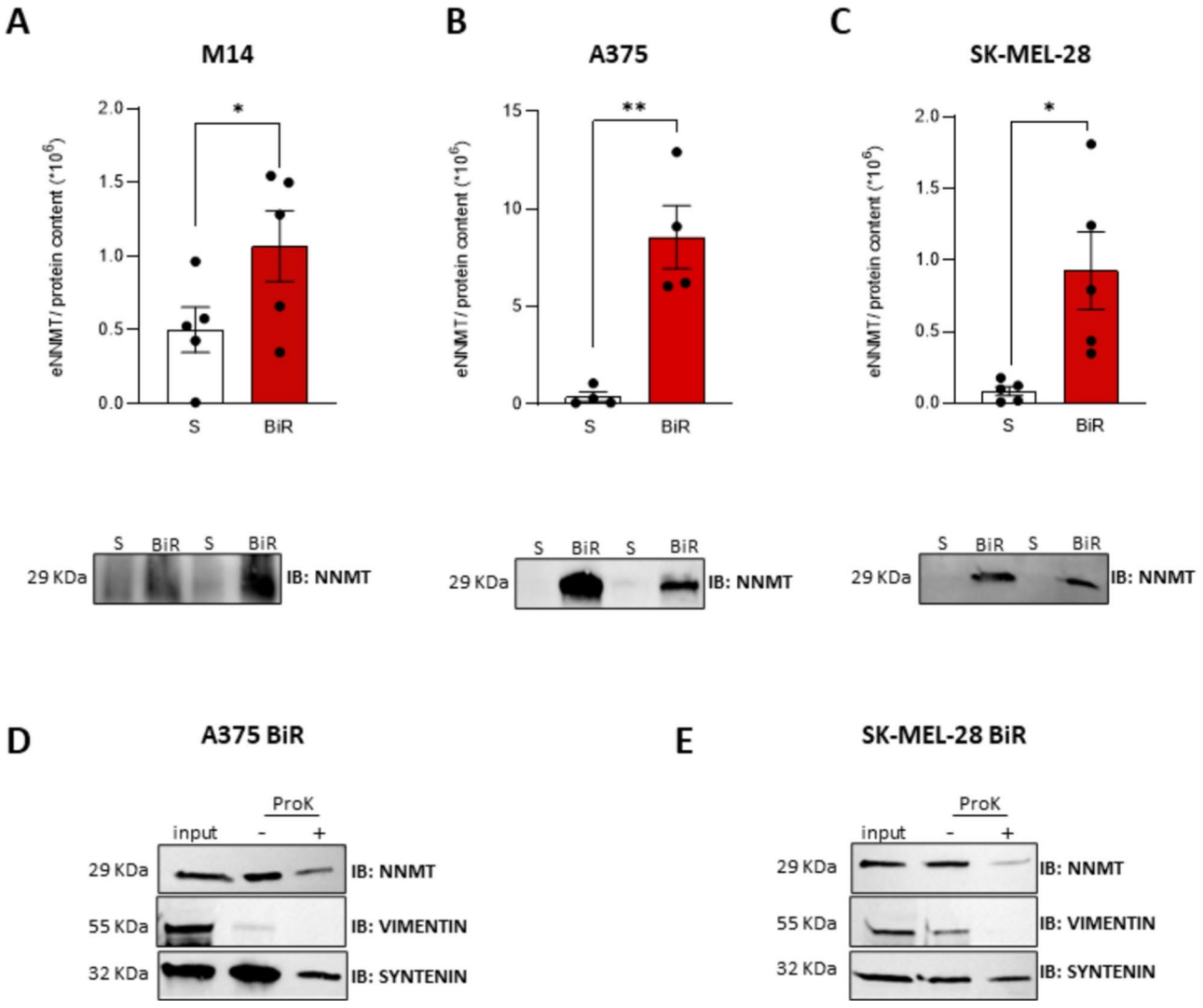

Fig. 4 eNNMT is abundant secreted either in exosomes or as a free protein in the supernatants (SN) derived from BiR MM cell lines. The presence of eNNMT was confirmed by western blot performed on 10× concentrated SN from M14 (**A**), A375 (**B**) and SK-MEL-28 (**C**) S and BiR variants in reducing conditions. Histograms show the cumulative data of $n = 4–5$ independent replicates. The amount of eNNMT detected was normalized over protein content in each replicate. Below the graphs are reported representative western blots. (**D**-**E**) SNs from A375 BiR (**D**) and SK-MEL28 BiR (**E**) cells were treated or not with Proteinase K (ProK, 100 ng/ml, 1 h at 37 °C) after ultracentrifugation (100,000 g for 70 min at 4 °C). SNs were concentrated 10x and was included an input condition: SN concentrated 10x before ultracentrifugation. NNMT expression was checked by western blot as reported in the representative images. Vimentin was used as free protein positive control, while Syntenin was used as exosomal protein control. Statistical significance was calculated using unpaired t-test. Data in the Figure are presented as the mean ± SEM. Significance was represented as: $*p \le 0.05$, $**p \le 0.01$

(p-value < 0.05) of 397 secreted proteins, in contrast to 382 downregulated ones (Supplementary Material 3). Importantly, we were able to confirm the presence of NAMPT (log_2FC 1.82 BiR vs. S) and NNMT (log_2FC 2.3) significantly enriched in SN from BiR cells (Fig. 5A-C). In addition to NAMPT and NNMT, we found up-regulated in SN from BiR cells also kynureninase (KYNU, log_2FC 2.26) and NAD(P)HX epimerase (NAXE, log_2FC 2.89) belonging to NAD network. Interestingly, the tryptophan (TRP) degradation (*de-novo* NAD biosynthetic route) along the kynurenine pathway (KP) plays a critical role in the regulation of immune response [94]. Among KP metabolites, kynurenine (KYN) production has been linked to cancer immune escape [95]. In melanoma, it has been demonstrated that the KP pathway mediates T-cell dysfunction [96].

Performing enrichment analysis, we identified an upregulation of translational and metabolic processes as purine, amino-acids, and carbon metabolism among the most significant (Fig. 5D). Moreover, an immune signature emerged, linked with TGF-β signaling, signaling by Rho GTPases, IL-12 signaling and neutrophil degranulation (Supplementary Material 3). Other interesting proteins belonging to these categories, found enriched in

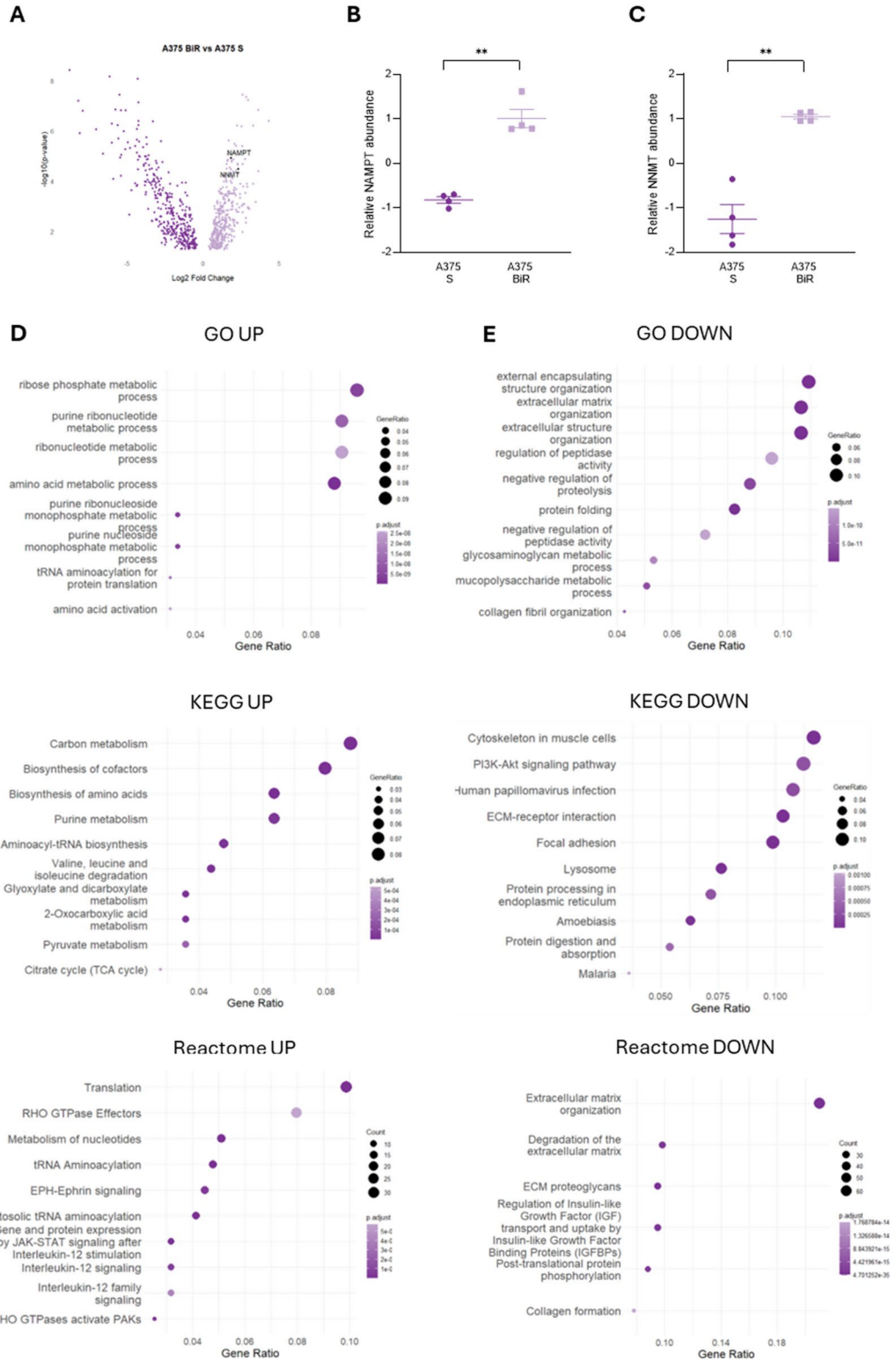

Fig. 5 NAMPT and NNMT are found in the secretome of A375 BiR cell line. (**A**) Volcano plot of significantly modulated proteins in A375 BiR compared with the respective sensitive A375 S cell line. Black dots with labels for NAMPT and NNMT are shown. Proteomics quantification of (**B**) NAMPT and (**C**) NNMT relative abundance in the supernatants of A375 S and BiR cells lines. Repeated measures one-way ANOVA was used to calculate statistical significance (**$p < 0.01$) between BiR and S cells. Dot plots of gene ontology GO (up), KEGG (middle) and Reactome (bottom) enrichment analysis of secreted proteins (**D**) up- or (**E**) downregulated in A375 BiR compared with A375 S cell lines. Dot size indicates gene count, and color represents adjusted p-value. Only significantly modulated proteins (p-value above 0.05) from four independent biological replicates were considered for the statistical analysis

SN from A375 BiR, are superoxide dismutase (SOD2), the most up-regulated protein with a log_2FC of 4.3, part of the superoxide dismutase family of redox enzymes that metabolize superoxide radicals into hydrogen peroxide. SOD2 expression increases in tumors, including in melanoma [97], as a mechanism to scavenge oxygen-reactive species (ROS); however, serum SOD2 levels may increase in melanoma patients and correlate with disease progression [98]. Interleukin-6 (IL-6, log_2FC 1.76), a cytokine involved in immune regulation, was previously detected in serum from melanoma patients [99]. NEDD8 ubiquitin-like modifier (NEDD8, log_2FC 2.43), a key element of the inflammasome caspase-1-dependent activation in primary macrophages [100]. We also identified different small Rab GTPases, conserved key regulators of membrane trafficking, also crucial for skin and hair pigmentation [100]. The most up-regulated is RAB6A (log_2FC 2.29) involved in the secretory pathway [101]. Several members of the serpin family [102], the most differentially expressed SERPINB2, log_2FC 3.45); the serine/threonine-protein kinase PAK2 (log_2FC 1.35), that plays an important role in cancer cell metastasis [103].

Downregulated terms point out a differential expression of proteins modulating the extracellular matrix formation and organization, collagen formation and integrin cell surface interactions (Fig. 5E, Supplementary Material 3). The rewiring of the proteins included in these terms could be associated with the metastatic process [104, 105]. Moreover, we also found cluster-differentiation (CD) proteins down-regulated, including CD44, CD59, CD58 and CD109. Among these, elevated soluble CD44 was previously associated with melanoma growth inhibition [106]; while a loss of CD58 expression confers immune evasion through multiple mechanisms, as recently reported [107].

NNMT correlates with NAMPT in melanoma patients and is more expressed in the BRAF-mutated ones, decreasing upon BRAFi/MEKi exposure

Herein, our objective is to elucidate the relationship between these two NAM-modulating enzymes, found overexpressed in resistant melanoma, with a subsequent focus on NNMT, which has been less extensively studied in this tumor model. Focusing on melanoma patients [Skin Cutaneous Melanoma (SKCM) TCGA cohort] we first analyzed the correlation between NAMPT and NNMT expression (metastatic samples $n = 368$). The analysis revealed a positive and significant correlation between the two NAM-modulating enzymes using both Spearman and Pearson tests (Fig. 6A). No correlation was detected in primary tumor samples (not shown). We confirmed the positive correlation (R or rho 0.3) also analyzing annotated melanoma cell lines ($n = 104$, filtered for primary disease "Skin Cancer" and subtype containing the term "Melanoma") in the cancer cell line encyclopedia (CCLE, Fig. 6B).

We previously knew that NAMPT expression increased in BRAF-mutated MM patients [28] and decreased following BRAFi treatment in vitro and in patients [23, 24, 26]. To highlight a possible association between NNMT expression and BRAF mutations we dissected the SKCM TCGA cohort (primary and metastatic samples) in BRAF wild-type (WT, $n = 235$) and BRAF-mutated (MUT, $n = 232$) patients. All annotated BRAF mutations were considered, with V600E being the most frequently represented, as expected. NNMT expression was significantly higher in patients harboring BRAF mutations (p-value = 4.99 e-05, Fig. 6C).

These data suggest a molecular connection between BRAF oncogenic signaling and the dysregulation of both NAMPT and NNMT enzyme. To corroborate this regulation, we treated the MM cell lines M14 BiR and A375 BiR with a combination "combo" of BRAF/MEK inhibitors (10 μM) for 24 h. Western blot analysis showed a down-regulation of NNMT protein expression in response to drugs treatment (Fig. 6D).

NNMT is positively associated with immune-related signature and signaling pathways in melanoma patients

By analyzing the gene expression profiles of these SKCM TCGA tumor samples using GSEA with respect to high vs. low NNMT expression (based on the median NNMT expression), we observed an increase in pro-inflammatory and immune-related signatures (including inflammation response, interferon response genes, humoral immune response, leucocyte migration, cell chemotaxis), and signaling pathways (MAP-kinase, NF-κB, chemokine-mediated signaling) correlated with higher NNMT expression (Fig. 7). Interestingly, high NNMT levels positively associated with neutrophils, granulocytes and myeloid cells migration (Supplementary Fig. 4), suggesting and increased immune infiltration and increased inflammatory status within the melanoma TME correlated with elevated NNMT. Moreover, we also observed a positive correlation between elevated NNMT and epithelial to mesenchymal transition and stemness (Supplementary Fig. 5A), as previously highlighted [29, 37], while a strong negative association with mRNA processing and cytoplasmic translation (Supplementary Fig. 5B).

Overall, these data indicate that, similarly to NAMPT, NNMT expression is associated with oncogenic BRAF signaling and shows a positive correlation with signaling and inflammatory signatures, suggesting its potential involvement in immune cell infiltration and modulation of the inflammatory response within the TME.

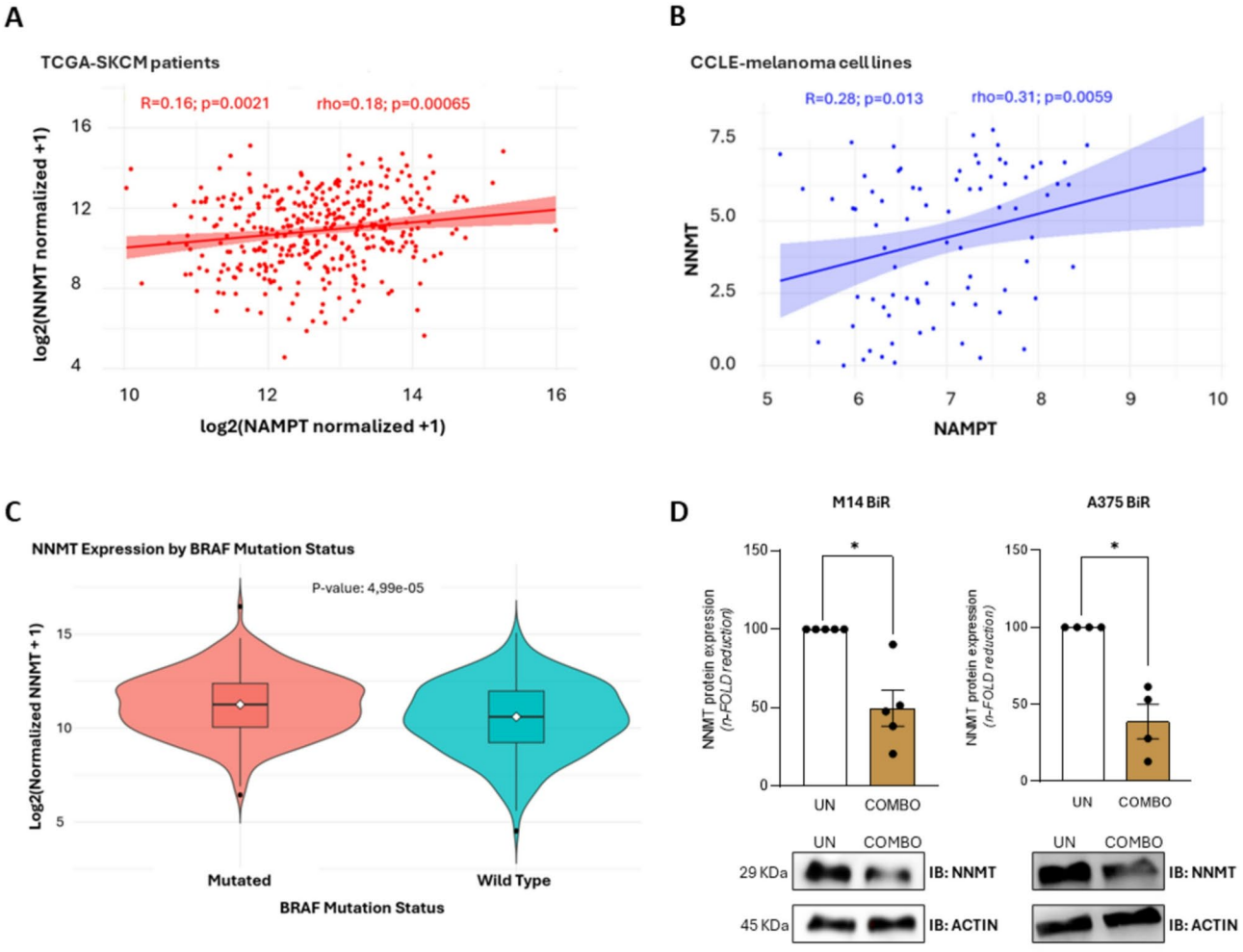

Fig. 6 *NAMPT* and *NNMT* are positively correlated and NNMT is more abundant in BRAF mutated MM patients. (**A-B**) Scatter plot correlating *NAMPT* and *NNMT*. Each dot represents a sample of the TCGA SKCM cohort, metastatic samples (**A**) or melanoma cell lines derived from CCLE dataset (**B**). Pearson (R) and Spearman (rho) correlations and p-value are shown. (**C**) *NNMT* expression (log2(normalized counts + 1)) was compared between *BRAF*-mutated and wild-type groups using the non-parametric Wilcoxon test. Data distributions were visualized using violin plots, reporting the *p-value* for statistical significance. (**D**) Analysis of NNMT expression in M14 BiR and A375 BiR after 24 h of treatment with the combination (combo) of Vemurafenib (10μM) and UO126 (10μM). M14 BiR $n = 5$, A375 BiR $n = 4$. Data are reported as n-fold compared to paired untreated condition for each replicate. Statistical significance was calculated using a paired t-test. Data in the Figure are presented as the mean ± SEM. Significance was represented as: $*p \leq 0.05$

Pharmacological inhibition or genetic knockdown of NNMT reduces BiR cells growth

To start to define the role of NNMT, previously unknown, as a driver of MM progression and drug resistance, we adopted two different strategies: (i) we used a NNMT pharmacological inhibitor (NNMTi, HY-131042) [63, 64] and (ii) we silenced NNMT in BiR cells transiently and stably using NNMT-specific siRNA and viral particles to express NNMT shRNA, respectively.

NNMT inhibition (~50 μM) led to a significant block of cell proliferation after 72 h as reported in Fig. 8A-C in all three BiR cell variants. NAMPT inhibitor (FK866 50 nM) was used a positive control of cell growth arrest [23]. A375 BiR cells are more sensitive to NNMT inhibition consistently with their higher expression of the enzyme. Colony formation assay was performed in A375 BiR and SK-MEL-28 BIR. Results showed a significant reduction of the colony-formation capability over a period of 10–12 days (Fig. 8D and Supplementary Fig. 6A) in both cell lines treated with NNMTi at 50 μM and more strongly with 100 μM. A375 BiR cells were more able to generate colonies compared with SK-MEL-28 BiR as depicted in representative images (Fig. 8D and Supplementary Fig. 6A), however the effect of NNMTi was comparable with a reduction of colonies of ~30% with NNMTi at 50 μM, increasing up to 70% with 100 μM. The impairment of cell growth was confirmed also by silencing *NNMT* gene as reported in Fig. 8E-F in M14 BiR cell line transiently transfected with siNNMT after 72 h, and in SK-MEL-28 BiR stably silenced for NNMT. Colony formation assay with SK-MEL-28 BiR stably silenced for

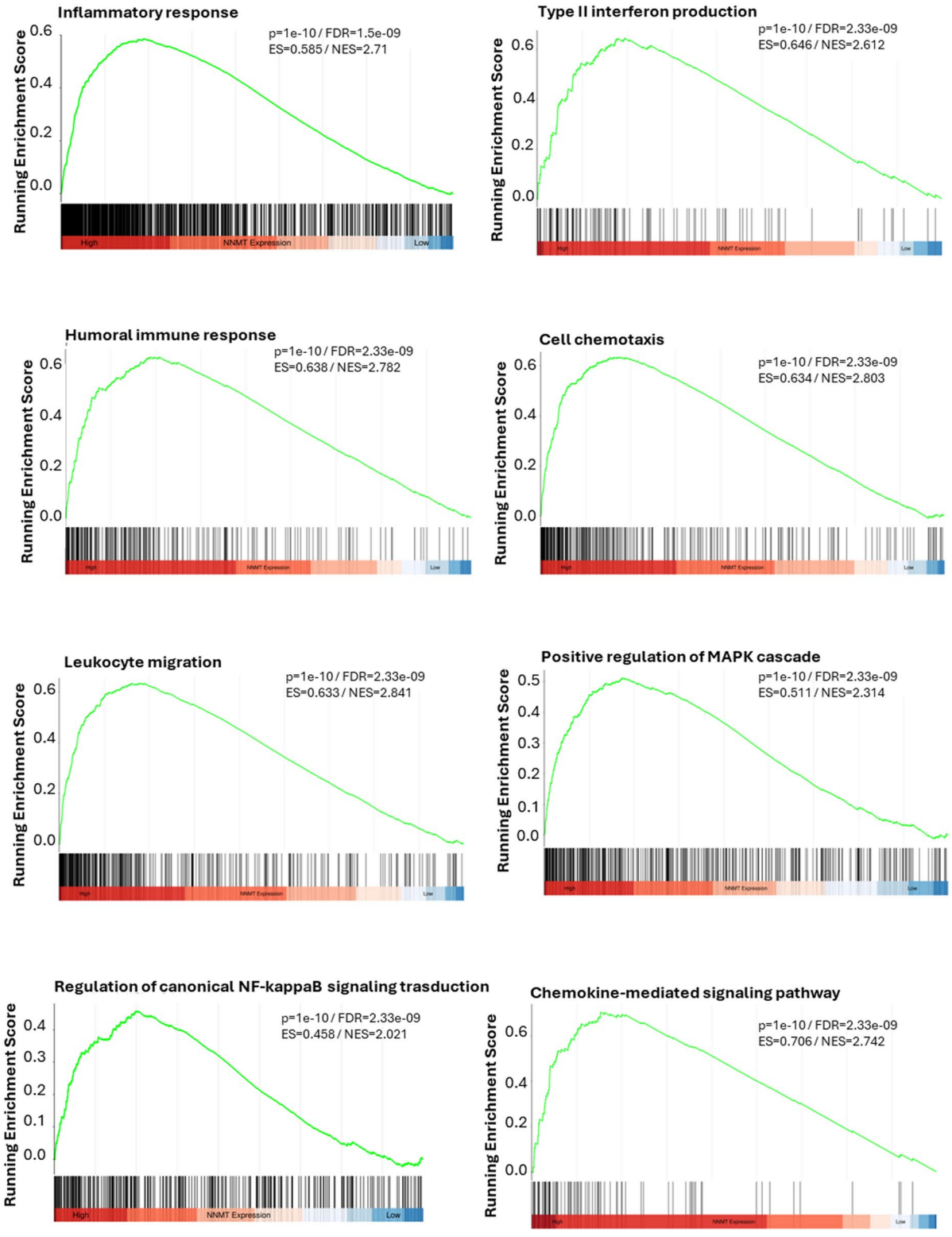

Fig. 7 NNMT correlates with inflammatory and immune-related categories. Gene set enrichment analysis (GSEA) for indicated pathways of gene expression data from TCGA melanoma transcriptomes. Samples were then stratified into two groups (*NNMT_high* and *NNMT_low*) based on the median *NNMT* expression. All the represented gene sets positively correlate with NNMT expression at a false discovery rate (FDR < 0.05). Enrichment score (ES), normalized enrichment score (NES)

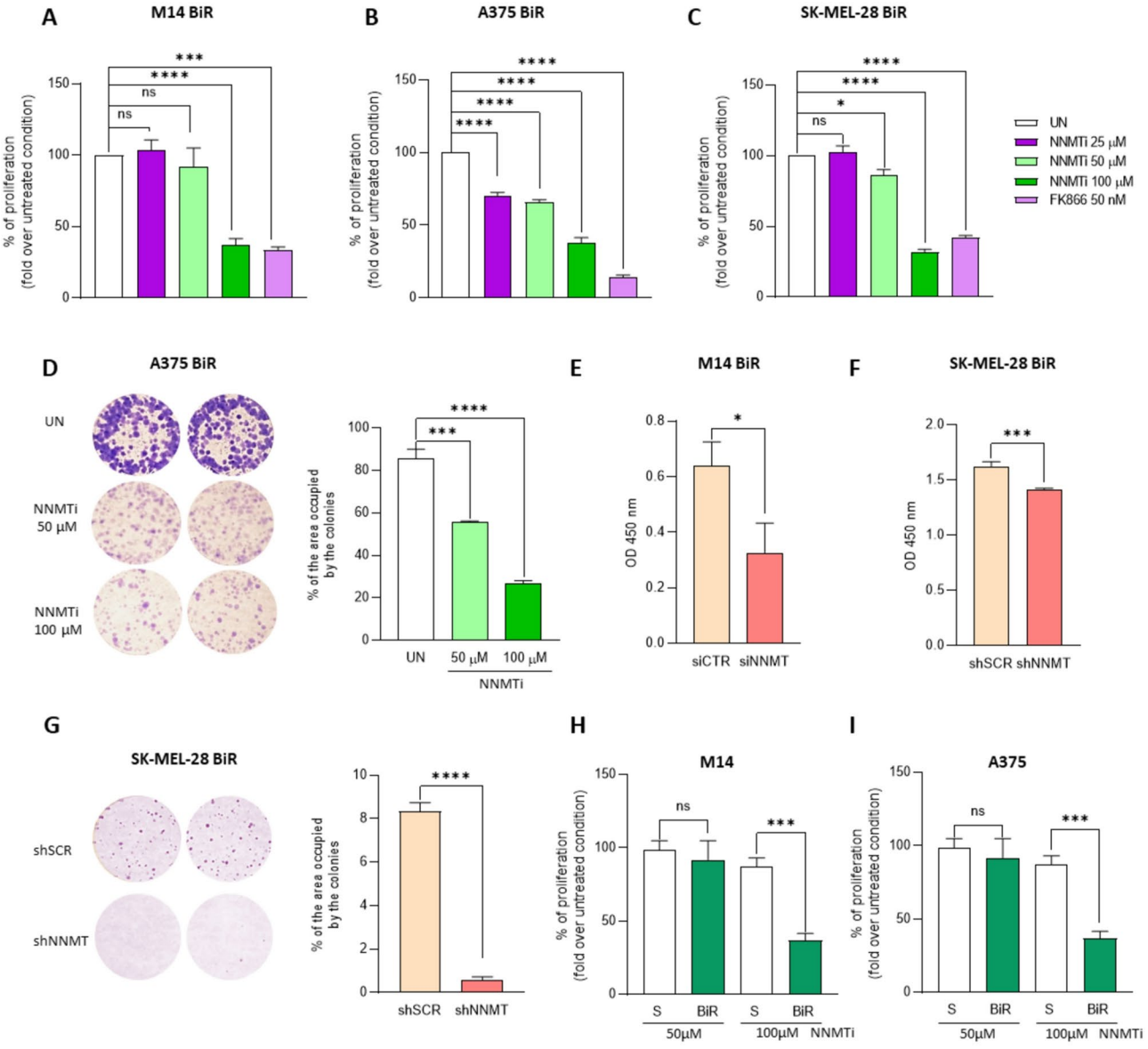

Fig. 8 Pharmacological inhibition or genetic knockdown of NNMT reduces BiR cells growth. (**A-C**) Short-term proliferation assay (CCK-8) evaluating the sensitivity of M14 BiR (**A**), A375 BiR (**B**) and SK-MEL-28 BiR (**C**) to the indicated increasing doses of NNMTi (72 h of treatment). NAMPT inhibitor FK866 (50 nM) was used as positive control of cell growth arrest. Data are from 3 independent experiments (each performed in triplicate) and are represented as % of proliferation (fold change over untreated condition). (**D**) Colony-forming ability (colony-forming units CFU) of A375 BiR treated with NNMTi (50–100 μM) in comparison with untreated cells for 12 days. Cells were stained with crystal violet and representative images are shown. On the right, histograms show the cumulative quantification of the percentage (%) area with colonies at the end of the 12-days period (2 independent experiments performed in triplicates). (**E**-**F**) CCK-8 assay comparing cell growth rate between M14 BiR transfected with siCRT vs. siNNMT (**E**) and between stably NNMT silenced SK-MEL-28 BiR and control cells (**F**). Data are from 2 independent experiments (each performed in triplicate) and are represented as absorbance 450 nm optical density (OD). (**G**) Representative images of CFU derived from stably shNNMT SK-MEL-28 BiR vs. shSCR cells maintained in culture for 12 days. On the right the cumulative graph representing the quantification of the percentage (%) area with colonies at the end of the 12-days period (3 independent experiments). **(H-I)** CCK-8 assay comparing sensitivity to NNMTi (50–100 μM, 72 h of treatment) of BiR vs. S cell lines. Data are represented as % of proliferation (fold change over untreated condition). Statistical significance was calculated using one-way ANOVA multiple comparisons (treatment groups compared with the untreated group) for A-D, unpaired t-test for E-I. Data in the Figure are presented as the mean ± SEM. Significance was represented as: $*p \leq 0.05$, $**p \leq 0.01$, $***p \leq 0.001$, $****p \leq 0.0001$

NNMT corroborated this significant reduction of cell growth (Fig. 8G). NNMT silencing in BiR cells was highlighted by RT-PCR and Western blot analysis (Supplementary Fig. 6B-C).

Selecting A375 and M14 we then compare the sensitivity of S and BiR cells to NNMTi. Data showed that A375 BiR were more sensitive than S variant to NNMTi (low dose of 50 μM, Fig. 8H), while in M14 cell line the

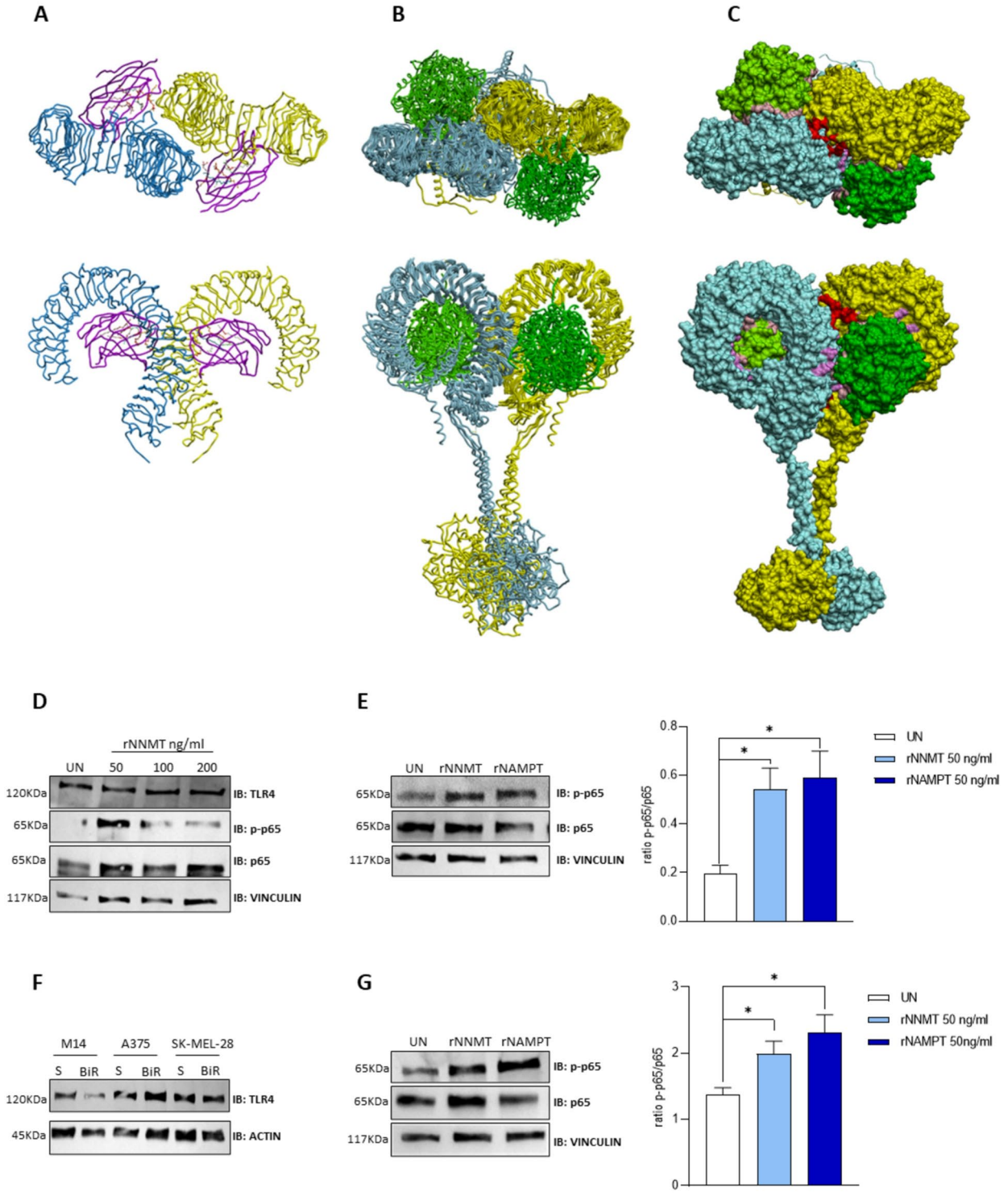

Fig. 9 (See legend on next page.)

increased sensitivity in BiR cells was appreciated at 100 μM (Fig. 8I).

Overall, these data suggest that NNMT inhibition in BiR cells could be a vulnerability of BRAF-resistant melanomas, supporting a previously uncharacterized function of this enzyme in BRAF/MEK resistance.

(See figure on previous page.)

Fig. 9 Putative NNMT: TLR4 complex model and eNNMT signaling function. NNMT-TLR4 complex was modeled with AI (AlphaFold Multimer) and compared with TLR4:MD2. (**A**) Crystal structure of TLR4-MD2 complex (PDB: RFXI) shown in worm representation. TLR4 subunits are colored blue and yellow, while MD-2 molecules are purple. (**B**) Superposition of five predicted NNMT-TLR4 complex models, illustrating structural convergence. (**C**) The highest-ranked NNMT-TLR4 model is depicted in a surface representation. NNMT-TLR4 interaction sites are highlighted in pink, while the TLR4 homodimerization interface is marked in red. NNMT molecules are green. The upper and lower panels depict the top and front views, respectively. (**D**) Western blot analysis of TLR4 and NF-kB p-p65 in differentiated THP-1 macrophages upon treatment (30 min) with increasing doses of rNNMT (50-100-200 ng/ml). (**E**) Representative western blot analysis of NF-kB p-p65 in differentiated THP-1 macrophages ($n=4$) upon treatment (30 min) with rNNMT and rNAMPT (both at 50 ng/ml). Cumulative graph on the right represents quantification of p-p65/p65, one-way ANOVA multiple comparisons. (**F**) Representative western blot analysis of basal expression of TLR4 in MM cells BiR/S variants. (**G**) Representative western blot analysis of NF-kB p-p65 in A375 BiR ($n=4$) upon treatment (30 min) with rNNMT and rNAMPT (both at 50 ng/ml). Cumulative graph on the right represents quantification of p-p65/p65, one-way ANOVA multiple comparisons. Data in the Figure are presented as the mean ± SEM. Significance was represented as: $^{*}p \leq 0.05$

eNNMT activates NF-κB signaling: exploring the possible involvement of TLR4

Based on the evidence that soluble NAD-biosynthetic enzymes (i.e., eNAMPT and eNAPRT) bind to TLR4 [44], we started to speculate that the newly identified eNNMT could bind TLR4 exerting a signaling function mediated by the engagement of the same receptor of eNAMPT/eNAPRT.

Using in silico methods, we investigated whether NNMT could form a stable complex with TLR4 to induce the homodimerization necessary for downstream signaling [108]. Given that human NNMT (~30 kDa) shares a molecular size comparable to the MD-2/LPS complex—a known ligand responsible for TLR4 activation—we hypothesized that hNNMT might act analogously by mimicking its mechanism. Specifically, we speculated that hNNMT could facilitate TLR4 dimerization and signaling by forming a heterotetrameric complex similar to MD-2/LPS. To investigate the possible structural arrangement of the heterotetrameric NNMT: TLR4 complex, we modelled it using AlphaFold Multimer [66]. The five predicted models consistently converged toward the same heterotetramer conformation, which resembles TLR4:MD2 (Fig. 9A-B). Figure 9C presents the highest-ranked model, which, based on the combined pTM + ipTM score of about 0.8, supports a reasonable prediction of the complex's overall fold and protein-protein interactions. Notably, each NNMT monomer (in green) makes electrostatic contact with both TLR4 subunits, potentially stabilizing TLR4 homodimerization. Our tetrameric NNMT: TLR4 model offers a plausible structural and mechanistic basis for their association. Lastly, we demonstrated that eNNMT is able to trigger NF-κB pathway, the main signaling activated by TLR4 binding, and previously reported for eNAMPT [43, 45, 109]. To do this we used commercial full-length and enzymatic active recombinant (r)NNMT protein (endotoxin-free). We decided first to exploit monocyte THP-1 model, as monocytes/macrophages are previously used to test eNAMPT signaling functions [43, 45, 109].

THP-1 cells can differentiate into macrophages in the presence of PMA and are a good model to test TLR4 agonists' activities, expressing high levels of the receptor [110] (Fig. 9D). Treatment of differentiated THP-1 with rNNMT for 30 min activated the NF-κB pathway, as determined by western blot analysis showing increased phosphorylation of the p65 subunit (Fig. 9D-E), evident with the low dose of rNNMT 50 ng/ml (Fig. 9D-E). rNAMPT treatment was included as positive control as known TLR4 ligand that robustly activates NF-κB signaling (Fig. 9E) [43, 45, 109].

Then we moved to validate our data in melanoma cells. We checked TLR4 expression in S and BiR MM cells. Western blot analysis reveals abundant expression of TLR4 on the surface of MM cells without significant differences in its expression in BiR cells compared to S cells (Fig. 9F). A375 BiR cells are highly TLR4-expressing cells, for this reason we used this cell line to repeat the treatment with rNNMT and rNAMPT, highlighting the activation of NF-κB pathway (Fig. 9G).

Overall, these data demonstrated, for the first time, that eNNMT triggers NF-κB activation in macrophages and in melanoma cells, supporting the idea that this signaling function could be mediated at least in part by TLR4 binding as reported by our prediction model of NNMT: TLR4 complex. Further studies will be necessary to verify this functional and physical interaction, as previously described for NAMPT [43, 109].

Discussion

Recent advancements in cancer research have increasingly focused on the analysis of tumor cell secretome and their microenvironment, both of which significantly influence tumor biology, including metastatic potential and resistance to therapy [4, 14, 111, 112]. Among the components of the tumor secretome, extracellular vesicles (EVs) have emerged as pivotal mediators of intercellular communication, contributing to tumor progression, metastasis, and therapeutic resistance by modulating the crosstalk between tumor and microenvironmental cells [113, 114]. These membrane-bound vesicles, secreted by virtually all cell types, are enriched with a wide array of molecular cargoes—such as proteins, lipids, and nucleic acids (small RNA, microRNA)—and have the capacity to exert paracrine effects both at local and systemic levels [115].

Accordingly, a comprehensive characterization of tumor secretome and EV-associated cargoes holds significant potential for the identification of novel biomarkers and therapeutic targets. Such insights may support the development of innovative treatment strategies aimed at reducing tumor burden and improving clinical outcomes.

Microenvironment-driven resistance to BRAF inhibition in melanoma patients is accompanied by broad changes in tumor secretome EV-associated cargoes, promoting the expansion and dissemination of drug-resistant clones and escape immune surveillance [4, 116, 117]. The secretome of BRAFi-resistant melanoma cells is rich in pro-tumor cytokines and angiogenic factors, including IL-8, IL-6, macrophage colony-stimulating factor (M-CSF) and transforming growth factor-β (TGF-β), thrombopoietin, vascular endothelial growth factor (VEGF) and leptin [5]. In addition, several enzymes were revealed by proteomic profiling of secretome derived from MM cell lines, including glyceraldehyde-3-phosphate dehydrogenase (GAPDH), α-enolase, pyruvate kinases isoenzymes, and triosephosphate isomerase [69]. Although primarily involved in cellular energy production, these enzymes have also been associated with non-metabolic functions when secreted [118, 119].

Consistently, in this work we showed that NAMPT and NNMT, the two rate-limiting enzymes of NAM metabolism inside cells, are present as soluble free-proteins and loaded into EVs preferentially in BRAFi-resistant melanoma cell lines.

The presence of NAMPT in EVs and/or exosomes was previously described in non-tumor and tumor contexts [70–77], but never in melanoma. eNAMPT, as soluble factor, was identified in several pathological conditions, including various inflammatory and metabolic disorders such as obesity, diabetes, arthritis, atherosclerosis, inflammatory bowel disease, lung injury, and cancer [18, 19, 44]. As recently reviewed by Semerena et al., eNAMPT is actively secreted by a wide variety of cell types through non-classical or unconventional pathways. This secretion is not a result of cell lysis or death; however, the precise mechanisms involved remain poorly understood [19]. Various signals can trigger NAMPT secretion, which can be broadly classified into three main categories: (i) cellular stress, (ii) nutritional and metabolic cues, and (iii) inflammatory stimuli. eNAMPT has been reported to exert multiples and diverse functions, which have been linked to its enzymatic activity as well as to its pro-inflammatory, pro-angiogenic, and adipocytokine roles [18, 19, 44]. eNAMPT can be viewed either as a pro-inflammatory cytokine or as an alarmin/DAMP. In general, eNAMPT appears as a modulator of innate immune pro-inflammatory programs, particularly in monocytes and macrophages. The enzymatic activity of the protein seems to be not required for these cytokine/DAMP activities of eNAMPT [18, 19, 45, 53, 109, 120]; on the contrary, eNAMPT exerts its extracellular functions by binding to one or more cell surface receptors. C-C chemokine receptor type 5 (CCR5) CCR5 and TLR4 were revealed as eNAMPT receptors [18, 19, 43, 109].

Among the various pathological conditions investigated, elevated levels of circulating eNAMPT are perhaps the most extensively studied in cancer. Increased eNAMPT concentrations have been reported across a wide spectrum of malignancies, including both solid tumors and hematological cancers [18, 19]. eNAMPT, secreted both by tumor and tumor-associated cells, is proposed to have a role in different hallmarks of cancer, promoting inflammation and cancer progression, and also as a component of the senescence-associated secretory phenotype (SASP) [18, 19, 121]. In melanoma, we and others previously demonstrated that NAMPT becomes a driver of targeted-therapy resistance modulating metabolic reprogramming [23–28]. eNAMPT is a cytokine-like protein released by MM cells, in vitro, and by MM patients [26, 78]. Audrito et al. in 2018 reported elevated eNAMPT levels in 113 patients with BRAF-mutated metastatic melanoma, compared to 50 patients with localized disease and 38 healthy donors. Circulating eNAMPT levels showed a direct correlation with markers of aggressive disease. Notably, eNAMPT concentrations decreased in response to BRAF/MEK inhibitor therapy but rose again upon disease progression/resistance [26].

The discovery that a second enzyme involved in NAM metabolism, i.e. NNMT, is concomitantly overexpressed upon the acquisition of BRAFi resistance in melanoma underscores a global rewiring of NAM metabolism as a mechanism of BRAFi resistance. NNMT increases at mRNA, intracellular, and extracellular protein levels. Although we cannot rule out technical inefficiencies in the sedimentation of particles with variable size and cellular heterogeneity, which may lead to secretomes of differing quality, the conclusive experimental evidence is that, using commonly adopted approaches for characterizing the cargo of extracellular vesicles, eNNMT could be detected both in its free form and as cargo within EVs.

The contribution of NNMT to cancer progression has been demonstrated across a range of malignancies; however, its functional role in cancer biology remains to be elucidated, especially as an extracellular protein. NNMT activity has been reported to promote tumor development and progression by directly and indirectly affecting epigenetic gene expression through the modulation of the intracellular SAM/SAH ratio, as well as by altering cancer metabolism [29–37]. Recently, it was also associated with acquired resistance to receptor-tyrosine kinase inhibitors (EGFR-TKI) in non-small cell lung cancer [64].

Circulating NNMT was uniquely identified as a free-soluble protein in NSCLC and colon cancer [46, 48] and

in exosomes from gastric cancer [47]. Different studies reported the overexpression and the function of NNMT in melanoma biology [38–42]. In this context, here we reported different novel findings, i.e., (i) NNMT overexpression in BRAF-mutated patients compared to the WT ones; (ii) increased levels of NNMT in BRAFi-resistant cells (mRNA and protein); (iii) increased amount of NNMT as soluble free-protein and in derived EVs in resistant cell lines; (iv) a positive correlation between NNMT and NAMPT, mirroring a dysregulation of NAM metabolism in melanoma secretome. Remarkably, (v) NNMT pharmacological inhibition or genetic silencing arrests BiR cells proliferation, more vulnerable to NNMT inhibition compared S cells. Lastly, (vi) we revealed a direct association of high NNMT levels with signaling and inflammatory signatures, demonstrating that recombinant NNMT triggers NF-kB activation, sharing this cytokine-like properties with NAMPT. We explored the possible involvement of TLR4 in NNMT-mediated NF-kB signaling activation modelling a prediction of tetrameric NNMT: TLR4 complex and offering a plausible structural and mechanistic basis for their association. Further studies will be necessary to verify the interaction between recombinant NNMT and the recombinant extracellular domain of TLR4 through surface plasmon resonance (SPR), as previously described for NAMPT [43, 109] and to discover structural determinants of eNNMT involved in TLR4 binding.

Overall, these data suggest the potential involvement of soluble NNMT in immune cell infiltration and modulation of the inflammatory response within the melanoma TME. This is a novel concept, recently discussed by Liu et al., who reported, by using a bioinformatics analysis, the correlation between NNMT and the infiltration of tumor-associated fibroblasts (CAFs) and macrophages (TAMs) in tumors [122]. Stromal NNMT expression was necessary and sufficient for functional aspects of CAF, and for secretion of cytokines and oncogenic extracellular matrix, supporting gastric and ovarian cancer migration, proliferation, and metastasis [123, 124]. Altogether, these findings underscore the multifaceted roles of NAMPT and NNMT in melanoma, with several open questions about their functional effects within the melanoma TME. The NAMPT/TLR4 signaling, as previously described [18, 19, 109, 125], may impact on tumor cells themselves and on immune cells, mainly macrophages, which express high levels of TLR4 [126]. The effect of NAMPT on macrophage recruitment and differentiation was previously reported [45]. Our signaling experiments and in silico reported NNMT: TLR4 binding, experimentally to be demonstrated, suggests very similar TLR4-mediated signaling also for eNNMT triggering NF-κB/inflammasome pathways. Therefore, we can hypothesize that NNMT could act as a new DAMP, a potent modulator of inflammatory responses, as previously reported for NAMPT and NAPRT [45].

Several issues remain to be addressed. First and foremost, it will be crucial to understand the relationship between NAMPT and NNMT in the regulation of NAD pathway homeostasis during the acquisition of targeted therapy resistance. It has been reported an evolutionary conserved kinetic interplay between these two NAM-metabolizing enzymes, impacting on NAM concentrations, and thereby also on NAD-consuming enzyme activities [127]. Secondly, it will be necessary to investigate the interconnection between the two soluble enzymes within the melanoma TME: our findings indicate that these are overexpressed, abundantly secreted and transferred via EVs, as a trait of resistance; however, the functional role needs to be clarified. Thirdly, it will be important to verify and define the mechanism of TLR4 engagement and the specific immune cells targeted by these enzymes/cytokines. Lastly, we do not forget the impact of metabolites (i.e., NAM, NMN, and MNA) produced by these enzymes within the TME [49, 50]. Future investigations will aim to resolve these open questions and to delineate a comprehensive resistance signature involving NAM-associated metabolites and enzymes.

Conclusion

In conclusion, the identification of NAMPT—and, unexpectedly, NNMT—overexpressed as intracellular proteins and abundantly released within EVs and as free proteins by resistant melanoma cells underscores the potential role of these moonlighting enzymes, involved in nicotinamide metabolism, as mediators of resistance to BRAF/MEK inhibitors. Their contribution may occur through tumor-intrinsic and possibly tumor microenvironment–mediated mechanisms. Moreover, the observed positive correlation between NNMT expression and gene signatures associated with pro-inflammatory signaling, immune cell migration, and chemokine-mediated pathways, together with the demonstration of NF-kB activation by exogenous NNMT exposure as well as our prediction of NNMT as a potential novel ligand for TLR4—the same receptor recognized by NAMPT—provide a compelling rationale for future studies aimed at elucidating the extracellular functions of NNMT in the remodeling of the tumor microenvironment. Lastly, targeting nicotinamide metabolism may represent a promising strategy to overcome drug resistance by modulating both tumor intrinsic processes and the multifactorial interactions between tumor cells and the host microenvironment.

Abbreviations

BiR	BRAF-inhibitor resistant cells
BRAF	B-Rapidly Accelerated Fibrosarcoma or V-Raf Murine Sarcoma Viral Oncogene Homolog B

BRAFi	BRAF Inhibitor
CCLE	Cancer Cell Line Encyclopedia
CCR5	C-C chemokine receptor type 5
CTLA-4	Cytotoxic T-Lymphocyte Antigen 4
DAMPs	Damage-Associated Molecular Patterns
DNMT1	DNA methyltransferase 1
eNAMPT	Extracellular Nicotinamide Phosphoribosyltransferase
eNAPRT	Extracellular Nicotinate Phosphoribosyltransferase
eNNMT	Extracellular Nicotinamide N-Methyltransferase
ER	endoplasmatic reticulum
EVs	Extracellular Vesicles
FDR	False Discovery Rate
GO	gene ontology
GSEA	Gene Set Enrichment Analysis
ICIs	Immune Checkpoint Inhibitors
IL-6	Interleukin-6
KP	kynurenine pathway
KYN	kynurenine
KYNU	kynureninase
MEKi	MEK Inhibitor
MM	metastatic melanoma
MNA	1-Methylnicotinamide
MS	Mass Spectrometry
NAD	Nicotinamide Adenine Dinucleotide
NADPH	Nicotinamide Adenine Dinucleotide Phosphate
NAM	Nicotinamide
NAMPT	Nicotinamide Phosphoribosyltransferase
NEDD8	NEDD8 ubiquitin like modifier
NF-KB	Nuclear Factor Kappa B
nLC-MS/MS	Nano Liquid Chromatography coupled with Tandem Mass Spectrometry
NNMT	Nicotinamide N-Methyltransferase
NSCLC	Non-Small Cell Lung Cancer
NTA	nanoparticle tracking analysis
PARPs	Poly (ADP-Ribose) Polymerases
PD-1	Programmed Cell Death Protein 1
PD-L1	Programmed Death-Ligand 1
PFA	Paraformaldehyde
ProK	proteinase K
pTM	predicted Template Model
qRT-PCR	Quantitative Real-Time Polymerase Chain Reaction
ROS	oxygen reactive species
S	BRAF-inhibitor sensitive cells
SAH	S-Adenosyl Homocysteine
SAM	S-Adenosyl Methionine
SGs	stress granule
SKCM	Skin Cutaneous Melanoma
SN	supernatants
SOD2	superoxide dismutase
STAT3	activator of transcription 3
TCGA	The Cancer Genome Atlas
TLR4	Toll-Like Receptor 4
TME	Tumor Microenvironment

Supplementary Information

The online version contains supplementary material available at https://doi.org/10.1186/s12964-025-02361-2.

Supplementary Material 1

Supplementary Material 2

Supplementary Material 3

Supplementary Material 4

Supplementary Material 5

Acknowledgements
We thank Romina Belli and Daniele Peroni from DeCIBIO's Proteomics and MS core facility at the University of Trento for performing the mass spectrometry analyses. The European Regional Development Fund (ERDF) 2014-2020 POR P.A. Trento is also acknowledged for supporting the Proteomics and MS core facility at the University of Trento.

Author contributions
V.A. designed experiments, interpreted results, and wrote the paper; B.G., I.F., A.C. performed experiments, analyzed data, and helped in the writing of the paper; L.A., A.PO., F.MA., A.M.T., N.T. and M.G. performed experiments; F.MA. and M.G. provided recombinant NAMPT protein; F.R. and F.M. performed TCGA/CCLE bioinformatic analysis; L.S. performed prediction analysis on NNMT:TLR4 binding; V.G.D. discussed the results; A.PR. designed MS experiments, discussed the results and revised the first draft of the paper. All authors read and approved the final manuscript.

Funding
This work was supported by Associazione Italiana Ricerca sul Cancro (AIRC), My First AIRC Grant–MFAG 2021 #24006 (to V.A.) and Investigator Grant-IG 21548 (to A.PR.), by 'Integrata' H2020 Marie Skłodowska-Curie Actions Innovative Training Networks (ITN) (813284 to A.PR.), by Associazione Italiana Leucemie (40104152 to A.PR.).

Data availability
The mass spectrometry proteomics data have been deposited to the ProteomeXchange Consortium via the PRIDE partner repository with the dataset identifier PXD063060 and 10.6019/PXD063060.

Declarations

Ethics approval and consent to participate
Not applicable.

Consent for publication
All authors read and are consent for the publication of this manuscript.

Competing interests
The authors declare no competing interests.

Author details
[1]Department of Science and Technological Innovation, University of Eastern Piedmont, Alessandria, ItalyViale Teresa Michel 11, 15121
[2]Department of Cellular, Computational and Integrative Biology (CIBIO), University of Trento, Trento, Italy
[3]SmartSeq s.r.l, Alessandria, Italy
[4]Division of Bioinformatics and Biochemistry, Department of Science and Engineering of Matter, Environment and Urban Planning, Polytechnic University of Marche, Ancona, Italy
[5]Department of Clinical Sciences, Polytechnic University of Marche, Ancona, Italy
[6]Department of Agriculture, Food and Environmental Sciences, Polytechnic University of Marche, Ancona, Italy
[7]Current address: Nuffield Department of Surgical Sciences, John Radcliffe Hospital, University of Oxford, Oxford OX3 9DU, UK

Received: 18 April 2025 / Accepted: 15 July 2025
Published online: 21 July 2025

References

1. de Visser KE, Joyce JA. The evolving tumor microenvironment: From cancer initiation to metastatic outgrowth. Cancer Cell. 2023;41:374–403. Available from: https://pubmed.ncbi.nlm.nih.gov/36917948/
2. Baghban R, Roshangar L, Jahanban-Esfahlan R, Seidi K, Ebrahimi-Kalan A, Jaymand M et al. Tumor microenvironment complexity and therapeutic implications at a glance. Cell Commun Signal. 2020;18. Available from: https://pubmed.ncbi.nlm.nih.gov/32264958/
3. Wang Q, Shao X, Zhang Y, Zhu M, Wang FXC, Mu J et al. Role of tumor microenvironment in cancer progression and therapeutic strategy. Cancer Med. 2023;12:11149–65. Available from: https://pubmed.ncbi.nlm.nih.gov/36807772/

4. Obenauf AC, Zou Y, Ji AL, Vanharanta S, Shu W, Shi H et al. Therapy-induced tumour secretomes promote resistance and tumour progression. Nature. 2015;520:368–72. Available from: https://pubmed.ncbi.nlm.nih.gov/25807485/
5. Barceló C, Sisó P, de la Rosa I, Megino-Luque C, Navaridas R, Maiques O et al. M-CSF as a therapeutic target in BRAFV600E melanoma resistant to BRAF inhibitors. Br J Cancer. 2022;127:1142–52. Available from: https://pubmed.ncbi.nlm.nih.gov/35725813/
6. Herraiz C, Jiménez-Cervantes C, Sánchez-Laorden B, García-Borrón JC. Functional interplay between secreted ligands and receptors in melanoma. Semin Cell Dev Biol. 2018;78:73–84. Available from: https://pubmed.ncbi.nlm.nih.gov/28676423/
7. Chakraborty P, Mukherjee C. The interplay of metabolic and epigenetic players in disease development. Biochem Biophys Res Commun. 2024;734. Available from: https://pubmed.ncbi.nlm.nih.gov/39217811/
8. Hugo W, Shi H, Sun L, Piva M, Song C, Kong X et al. Non-genomic and Immune Evolution of Melanoma Acquiring MAPKi Resistance. Cell. 2015;162:1271–85. Available from: https://pubmed.ncbi.nlm.nih.gov/26359985/
9. Arozarena I, Wellbrock C. Phenotype plasticity as enabler of melanoma progression and therapy resistance. Nat Rev Cancer. 2019;19:377–91. Available from: https://pubmed.ncbi.nlm.nih.gov/31209265/
10. Bai X, Fisher DE, Flaherty KT. Cell-state dynamics and therapeutic resistance in melanoma from the perspective of MITF and IFNγ pathways. Nat Rev Clin Oncol. 2019;16:549–62. Available from: https://pubmed.ncbi.nlm.nih.gov/30967646/
11. Abildgaard C, Guldberg P. Molecular drivers of cellular metabolic reprogramming in melanoma. Trends Mol Med. 2015;21:164–71. Available from: https://pubmed.ncbi.nlm.nih.gov/25618774/
12. Ramapriyan R, Caetano MS, Barsoumian HB, Mafra ACP, Zambalde EP, Menon H et al. Altered cancer metabolism in mechanisms of immunotherapy resistance. Pharmacol Ther. 2019;195:162–71. Available from: https://pubmed.ncbi.nlm.nih.gov/30439456/
13. A targeted therapy-driven tumor secretome underlies drug resistance. Cancer Discov. 2015;5:OF8. Available from: http://cancerdiscovery/article/5/5/OF8/5109/A-Targeted-Therapy-Driven-Tumor-Secretome
14. Yang J, Tang S, Saba NF, Shay C, Teng Y. Tumor secretome shapes the immune landscape during cancer progression. J Exp Clin Cancer Res. 2025;44:47. Available from: https://pubmed.ncbi.nlm.nih.gov/39930476/
15. Migaud ME, Ziegler M, Baur JA. Regulation of and challenges in targeting NAD + metabolism. Nat Rev Mol Cell Biol. 2024;25. Available from: https://pubmed.ncbi.nlm.nih.gov/39026037/
16. Chiarugi A, Dölle C, Felici R, Ziegler M. The NAD metabolome–a key determinant of cancer cell biology. Nat Rev Cancer. 2012;12:741–52. Available from: https://pubmed.ncbi.nlm.nih.gov/23018234/
17. Garten A, Schuster S, Penke M, Gorski T, De Giorgis T, Kiess W. Physiological and pathophysiological roles of NAMPT and NAD metabolism. Nat Rev Endocrinol. 2015;11:535–46. Available from: https://pubmed.ncbi.nlm.nih.gov/26215259/
18. Gasparrini M, Audrito V, NAMPT. A critical driver and therapeutic target for cancer. Int J Biochem Cell Biol. 2022;145. Available from: https://pubmed.ncbi.nlm.nih.gov/35219878/
19. Semerena E, Nencioni A, Masternak K. Extracellular nicotinamide phosphoribosyltransferase: role in disease pathophysiology and as a biomarker. Front Immunol. 2023;14. Available from: https://pubmed.ncbi.nlm.nih.gov/37915565/
20. Galli U, Colombo G, Travelli C, Tron GC, Genazzani AA, Grolla AA. Recent Advances in NAMPT Inhibitors: A Novel Immunotherapic Strategy. Front Pharmacol. 2020;11. Available from: https://pubmed.ncbi.nlm.nih.gov/32477131/
21. Ghanem MS, Caffa I, Monacelli F, Nencioni A. Inhibitors of NAD + Production in Cancer Treatment: State of the Art and Perspectives. Int J Mol Sci. 2024;25. Available from: https://pubmed.ncbi.nlm.nih.gov/38396769/
22. Chowdhry S, Zanca C, Rajkumar U, Koga T, Diao Y, Raviram R et al. NAD metabolic dependency in cancer is shaped by gene amplification and enhancer remodelling. Nature. 2019;569:570–5. Available from: https://pubmed.ncbi.nlm.nih.gov/31019297/
23. Audrito V, Managò A, La Vecchia S, Zamporlini F, Vitale N, Baroni G et al. Nicotinamide Phosphoribosyltransferase (NAMPT) as a Therapeutic Target in BRAF-Mutated Metastatic Melanoma. J Natl Cancer Inst. 2018;110. Available from: https://pubmed.ncbi.nlm.nih.gov/29309612/
24. Ohanna M, Cerezo M, Nottet N, Bille K, Didier R, Beranger G et al. Pivotal role of NAMPT in the switch of melanoma cells toward an invasive and drug-resistant phenotype. Genes Dev. 2018;32:448–61. Available from: https://pubmed.ncbi.nlm.nih.gov/29567766/
25. Audrito V, Messana VG, Moiso E, Vitale N, Arruga F, Brandimarte L et al. NAMPT Over-Expression Recapitulates the BRAF Inhibitor Resistant Phenotype Plasticity in Melanoma. Cancers (Basel). 2020;12:1–22. Available from: https://pubmed.ncbi.nlm.nih.gov/33419372/
26. Audrito V, Managò A, Zamporlini F, Rulli E, Gaudino F, Madonna G et al. Extracellular nicotinamide phosphoribosyltransferase (eNAMPT) is a novel marker for patients with BRAF-mutated metastatic melanoma. Oncotarget. 2018;9:18997–9005. Available from: https://pubmed.ncbi.nlm.nih.gov/29721178/
27. Audrito V, Managò A, Gaudino F, Deaglio S. Targeting metabolic reprogramming in metastatic melanoma: The key role of nicotinamide phosphoribosyltransferase (NAMPT). Semin Cell Dev Biol. 2020;98:192–201. Available from: https://pubmed.ncbi.nlm.nih.gov/31059816/
28. Audrito V, Moiso E, Ugolini F, Messana VG, Brandimarte L, Manfredonia I et al. Tumors carrying BRAF-mutations over-express NAMPT that is genetically amplified and possesses oncogenic properties. J Transl Med. 2022;20:1–13. Available from: https://translational-medicine.biomedcentral.com/articles/https://doi.org/10.1186/s12967-022-03315-9
29. Wang W, Yang C, Wang T, Deng H. Complex roles of nicotinamide N-methyltransferase in cancer progression. Cell Death Dis. 2022;13. Available from: https://pubmed.ncbi.nlm.nih.gov/35338115/
30. Roberti A, Fernández AF, Fraga MF. Nicotinamide N-methyltransferase: At the crossroads between cellular metabolism and epigenetic regulation. Mol Metab. 2021;45. Available from: https://pubmed.ncbi.nlm.nih.gov/33453420/
31. Loring HS, Thompson PR. Kinetic Mechanism of Nicotinamide N-Methyltransferase. Biochemistry. 2018;57:5524–32. Available from: https://pubmed.ncbi.nlm.nih.gov/30148963/
32. Gao Y, Martin NI, van Haren MJ. Nicotinamide N-methyl transferase (NNMT): An emerging therapeutic target. Drug Discov Today. 2021;26:2699–706. Available from: https://pubmed.ncbi.nlm.nih.gov/34029690/
33. Sibani S, Melnyk S, Pogribny IP, Wang W, Hiou-Tim F, Deng L et al. Studies of methionine cycle intermediates (SAM, SAH), DNA methylation and the impact of folate deficiency on tumor numbers in Min mice. Carcinogenesis. 2002;23:61–5. Available from: https://pubmed.ncbi.nlm.nih.gov/11756224/
34. Ducker GS, Rabinowitz JD. One-Carbon Metabolism in Health and Disease. Cell Metab. 2017;25:27–42. Available from: https://pubmed.ncbi.nlm.nih.gov/27641100/
35. Ulanovskaya OA, Zuhl AM, Cravatt BF. NNMT promotes epigenetic remodeling in cancer by creating a metabolic methylation sink. Nat Chem Biol. 2013;9:300–6. Available from: https://pubmed.ncbi.nlm.nih.gov/23455543/
36. Lu XM, Long H. Nicotinamide N-methyltransferase as a potential marker for cancer. Neoplasma. 2018;65:656–63. Available from: https://pubmed.ncbi.nlm.nih.gov/29940773/
37. Parsons RB, Facey PD. Nicotinamide N-Methyltransferase: An Emerging Protagonist in Cancer Macro(r)evolution. Biomolecules. 2021;11. Available from: https://pubmed.ncbi.nlm.nih.gov/34680055/
38. Campagna R, Pozzi V, Sartini D, Salvolini E, Brisigotti V, Molinelli E et al. Beyond Nicotinamide Metabolism: Potential Role of Nicotinamide N-Methyltransferase as a Biomarker in Skin Cancers. Cancers (Basel). 2021;13. Available from: https://pubmed.ncbi.nlm.nih.gov/34638427/
39. Ganzetti G, Sartini D, Campanati A, Rubini C, Molinelli E, Brisigotti V et al. Nicotinamide N-methyltransferase: potential involvement in cutaneous malignant melanoma. Melanoma Res. 2018;28:82–8. Available from: https://pubmed.ncbi.nlm.nih.gov/29420365/
40. Mascitti M, Santarelli A, Sartini D, Rubini C, Colella G, Salvolini E et al. Analysis of nicotinamide N-methyltransferase in oral malignant melanoma and potential prognostic significance. Melanoma Res. 2019;29:151–6. Available from: https://pubmed.ncbi.nlm.nih.gov/30431528/
41. Sartini D, Molinelli E, Pozzi V, Campagna R, Salvolini E, Rubini C et al. Immunohistochemical expression of nicotinamide N-methyltransferase in lymph node metastases from cutaneous malignant melanoma. Hum Cell [Internet]. 2023 [cited 2025 Apr 8];36:480–2. Available from: https://pubmed.ncbi.nlm.nih.gov/36151433/
42. Campagna R, Salvolini E, Pompei V, Pozzi V, Salvucci A, Molinelli E et al. Nicotinamide N-methyltransferase gene silencing enhances chemosensitivity of melanoma cell lines. Pigment Cell Melanoma Res. 2021;34:1039–48. Available from: https://pubmed.ncbi.nlm.nih.gov/34018676/

43. Camp SM, Ceco E, Evenoski CL, Danilov SM, Zhou T, Chiang ET et al. Unique Toll-Like Receptor 4 Activation by NAMPT/PBEF Induces NFκB Signaling and Inflammatory Lung Injury. Sci Rep. 2015;5. Available from: https://pubmed.ncbi.nlm.nih.gov/26272519/
44. Audrito V, Messana VG, Deaglio S. NAMPT and NAPRT: Two Metabolic Enzymes With Key Roles in Inflammation. Front Oncol. 2020;10. Available from: https://pubmed.ncbi.nlm.nih.gov/32266141/
45. Managò A, Audrito V, Mazzola F, Sorci L, Gaudino F, Gizzi K et al. Extracellular nicotinate phosphoribosyltransferase binds Toll like receptor 4 and mediates inflammation. Nature Communications. 2019;10:1–14. Available from: https://www.nature.com/articles/s41467-019-12055-2
46. Tomida M, Mikami I, Takeuchi S, Nishimura H, Akiyama H. Serum levels of nicotinamide N-methyltransferase in patients with lung cancer. J Cancer Res Clin Oncol. 2009;135:1223–9. Available from: https://pubmed.ncbi.nlm.nih.gov/19242722/
47. Zhu AK, Shan YQ, Zhang J, Liu XC, Ying RC, Kong WC. Exosomal NNMT from peritoneum lavage fluid promotes peritoneal metastasis in gastric cancer. Kaohsiung J Med Sci. 2021;37:305–13. Available from: https://pubmed.ncbi.nlm.nih.gov/33508890/
48. Roeßler M, Rollinger W, Palme S, Hagmann ML, Berndt P, Engel AM et al. Identification of nicotinamide N-methyltransferase as a novel serum tumor marker for colorectal cancer. Clin Cancer Res. 2005;11:6550–7. Available from: https://pubmed.ncbi.nlm.nih.gov/16166432/
49. Jiang Y, Wang Y, Chen G, Sun F, Wu Q, Huang Q et al. Nicotinamide metabolism face-off between macrophages and fibroblasts manipulates the microenvironment in gastric cancer. Cell Metab. 2024;36:1806–1822.e11. Available from: https://pubmed.ncbi.nlm.nih.gov/38897198/
50. Audrito V, Messana VG, Brandimarte L, Deaglio S. The Extracellular NADome Modulates Immune Responses. Front Immunol. 2021;12. Available from: https://pubmed.ncbi.nlm.nih.gov/34421911/
51. Kilgour MK, MacPherson S, Zacharias LG, Ellis AE, Sheldon RD, Liu EY et al. 1-Methylnicotinamide is an immune regulatory metabolite in human ovarian cancer. Sci Adv. 2021;7. Available from: https://pubmed.ncbi.nlm.nih.gov/33523930/
52. Ponzone L, Audrito V, Landi C, Moiso E, Levra Levron C, Ferrua S et al. RICTOR/mTORC2 downregulation in BRAFV600E melanoma cells promotes resistance to BRAF/MEK inhibition. Mol Cancer. 2024;23. Available from: https://pubmed.ncbi.nlm.nih.gov/38755661/
53. Audrito V, Serra S, Brusa D, Mazzola F, Arruga F, Vaisitti T et al. Extracellular nicotinamide phosphoribosyltransferase (NAMPT) promotes M2 macrophage polarization in chronic lymphocytic leukemia. Blood. 2015;125:111–23. Available from: https://pubmed.ncbi.nlm.nih.gov/25368373/
54. Cvjetkovic A, Jang SC, Konečná B, Höög JL, Sihlbom C, Lässer C et al. Detailed Analysis of Protein Topology of Extracellular Vesicles-Evidence of Unconventional Membrane Protein Orientation. Sci Rep. 2016;6:1–12. Available from: https://www.nature.com/articles/srep36338
55. Paré B, Deschênes LT, Pouliot R, Dupré N, Gros-Louis F. An Optimized Approach to Recover Secreted Proteins from Fibroblast Conditioned-Media for Secretomic Analysis. Front Cell Neurosci. 2016;10. Available from: https://pubmed.ncbi.nlm.nih.gov/27064649/
56. Hughes CS, Moggridge S, Müller T, Sorensen PH, Morin GB, Krijgsveld J. Single-pot, solid-phase-enhanced sample preparation for proteomics experiments. Nat Protoc. 2019;14:68–85. Available from: https://pubmed.ncbi.nlm.nih.gov/30464214/
57. Waas M, Pereckas M, Jones Lipinski RA, Ashwood C, Gundry RL. SP2: Rapid and Automatable Contaminant Removal from Peptide Samples for Proteomic Analyses. J Proteome Res. 2019;18:1644–56. Available from: https://pubmed.ncbi.nlm.nih.gov/30795648/
58. Chiva C, Olivella R, Borràs E, Espadas G, Pastor O, Solé A et al. QCloud: A cloud-based quality control system for mass spectrometry-based proteomics laboratories. PLoS One. 2018;13. Available from: https://pubmed.ncbi.nlm.nih.gov/29324744/
59. Zhu Y, Orre LM, Tran YZ, Mermelekas G, Johansson HJ, Malyutina A et al. DEqMS: A Method for Accurate Variance Estimation in Differential Protein Expression Analysis. Mol Cell Proteomics. 2020;19:1047–57. Available from: https://pubmed.ncbi.nlm.nih.gov/32205417/
60. Kim HJ, Kim T, Hoffman NJ, Xiao D, James DE, Humphrey SJ et al. PhosR enables processing and functional analysis of phosphoproteomic data. Cell Rep. 2021;34. Available from: https://pubmed.ncbi.nlm.nih.gov/33626354/
61. Xie Z, Bailey A, Kuleshov MV, Clarke DJB, Evangelista JE, Jenkins SL et al. Gene Set Knowledge Discovery with Enrichr. Curr Protoc. 2021;1:e90. Available from: https://onlinelibrary.wiley.com/doi/full/https://doi.org/10.1002/cpz1.90
62. Perez-Riverol Y, Bandla C, Kundu DJ, Kamatchinathan S, Bai J, Hewapathirana S et al. The PRIDE database at 20 years: 2025 update. Nucleic Acids Res. 2025;53:D543–53. Available from: https://doi.org/10.1093/nar/gkae1011
63. Wang Z, Wang Q, Chen C, Zhao X, Wang H, Xu L et al. NNMT enriches for AQP5 + cancer stem cells to drive malignant progression in early gastric cardia adenocarcinoma. Gut. 2023;73:63–77. Available from: https://pubmed.ncbi.nlm.nih.gov/36977555/
64. Dai J, Lu X, Zhang C, Qu T, Li W, Su J et al. NNMT promotes acquired EGFR-TKI resistance by forming EGR1 and lactate-mediated double positive feedback loops in non-small cell lung cancer. Mol Cancer. 2025;24:1–19. Available from: https://molecular-cancer.biomedcentral.com/articles/https://doi.org/10.1186/s12943-025-02285-y
65. Evans R, O'Neill M, Pritzel A, Antropova N, Senior A, Green T et al. Protein complex prediction with AlphaFold-Multimer. 2021. Available from: https://europepmc.org/article/ppr/ppr403752
66. Jumper J, Evans R, Pritzel A, Green T, Figurnov M, Ronneberger O et al. Highly accurate protein structure prediction with AlphaFold. Nature. 2021;596:583–9. Available from: https://pubmed.ncbi.nlm.nih.gov/34265844/
67. Mirdita M, Schütze K, Moriwaki Y, Heo L, Ovchinnikov S, Steinegger M. ColabFold: making protein folding accessible to all. Nat Methods. 2022;19:679–82. Available from: https://pubmed.ncbi.nlm.nih.gov/35637307/
68. Neves MAC, Totrov M, Abagyan R. Docking and scoring with ICM: the benchmarking results and strategies for improvement. J Comput Aided Mol Des. 2012;26:675–86. Available from: https://pubmed.ncbi.nlm.nih.gov/22569591/
69. Rocco M, Malorni L, Cozzolino R, Palmieri G, Rozzo C, Manca A et al. Proteomic profiling of human melanoma metastatic cell line secretomes. J Proteome Res. 2011;10:4709–14. Available from: https://pubmed.ncbi.nlm.nih.gov/21815687/
70. Yoshida M, Satoh A, Lin JB, Mills KF, Sasaki Y, Rensing N et al. Extracellular Vesicle-Contained eNAMPT Delays Aging and Extends Lifespan in Mice. Cell Metab. 2019;30:329–342.e5. Available from: https://pubmed.ncbi.nlm.nih.gov/31204283/
71. Deng Y, Duan R, Ding W, Gu Q, Liu M, Zhou J et al. Astrocyte-derived exosomal nicotinamide phosphoribosyltransferase (Nampt) ameliorates ischemic stroke injury by targeting AMPK/mTOR signaling to induce autophagy. Cell Death Dis. 2022;13. Available from: https://pubmed.ncbi.nlm.nih.gov/36539418/
72. Lu YB, Chen CX, Huang J, Tian YX, Xie X, Yang P et al. Nicotinamide phosphoribosyltransferase secreted from microglia via exosome during ischemic injury. J Neurochem. 2019;150:723–37. Available from: https://pubmed.ncbi.nlm.nih.gov/31269239/
73. Wu G, Su Q, Li J, Xue C, Zhu J, Cai Q et al. NAMPT encapsulated by extracellular vesicles from young adipose-derived mesenchymal stem cells treated tendinopathy in a One-Stone-Two-Birds manner. J Nanobiotechnology. 2023;21. Available from: https://pubmed.ncbi.nlm.nih.gov/36604715/
74. Chong MC, Silva A, James PF, Wu SSX, Howitt J. Exercise increases the release of NAMPT in extracellular vesicles and alters NAD + activity in recipient cells. Aging Cell. 2022;21. Available from: https://pubmed.ncbi.nlm.nih.gov/35661560/
75. Ni J, Zhang J, Liu J, Fan L, Lin X, Yu H et al. Exosomal NAMPT from chronic lymphocytic leukemia cells orchestrate monocyte survival and phenotype under endoplasmic reticulum stress. Hematol Oncol. 2023;41:61–70. Available from: https://pubmed.ncbi.nlm.nih.gov/36321597/
76. Panizza E, Regalado BD, Wang F, Nakano I, Vacanti NM, Cerione RA et al. Proteomic analysis reveals microvesicles containing NAMPT as mediators of radioresistance in glioma. Life Sci Alliance. 2023;6. Available from: https://pubmed.ncbi.nlm.nih.gov/37037593/
77. Rizk NI, Kassem DH, Abulsoud AI, AbdelHalim S, Yasser MB, Kamal MM et al. Revealing the role of serum exosomal novel long non-coding RNA NAMPT-AS as a promising diagnostic/prognostic biomarker in colorectal cancer patients. Life Sci. 2024;352. Available from: https://pubmed.ncbi.nlm.nih.gov/38901687/
78. Grolla AA, Torretta S, Gnemmi I, Amoruso A, Orsomando G, Gatti M et al. Nicotinamide phosphoribosyltransferase (NAMPT/PBEF/visfatin) is a tumoural cytokine released from melanoma. Pigment Cell Melanoma Res. 2015;28:718–29. Available from: https://onlinelibrary.wiley.com/doi/full/https://doi.org/10.1111/pcmr.12420
79. Audrito V, Serra S, Stingi A, Orso F, Gaudino F, Bologna C et al. PD-L1 up-regulation in melanoma increases disease aggressiveness and is mediated through miR-17-5p. Oncotarget. 2017;8:15894–911. Available from: https://www.oncotarget.com/article/15213/text/

80. Gurrieri E, Carradori G, Roccuzzo M, Pancher M, Peroni D, Belli R et al. CD81-guided heterologous EVs present heterogeneous interactions with breast cancer cells. J Biomed Sci. 2024;31:92. Available from: https://pubmed.ncbi.nlm.nih.gov/39402557/
81. Wang X, Chai Y, Quan Y, Wang J, Song J, Zhou W et al. NPM1 inhibits tumoral antigen presentation to promote immune evasion and tumor progression. J Hematol Oncol. 2024;17:97. Available from: https://pubmed.ncbi.nlm.nih.gov/39402629/
82. Qin G, Wang X, Ye S, Li Y, Chen M, Wang S et al. NPM1 upregulates the transcription of PD-L1 and suppresses T cell activity in triple-negative breast cancer. Nat Commun. 2020;11. Available from: https://pubmed.ncbi.nlm.nih.gov/32245950/
83. Zhou H, Luo J, Mou K, Peng L, Li X, Lei Y et al. Stress granules: functions and mechanisms in cancer. Cell Biosci. 2023;13. Available from: https://pubmed.ncbi.nlm.nih.gov/37179344/
84. Franchini DM, Lanvin O, Tosolini M, Patras de Campaigno E, Cammas A, Péricart S et al. Microtubule-Driven Stress Granule Dynamics Regulate Inhibitory Immune Checkpoint Expression in T Cells. Cell Rep. 2019;26:94–107.e7. Available from: https://pubmed.ncbi.nlm.nih.gov/30605689/
85. Unterholzner L, Keating SE, Baran M, Horan KA, Jensen SB, Sharma S et al. IFI16 is an innate immune sensor for intracellular DNA. Nat Immunol. 2010;11:997–1004. Available from: https://pubmed.ncbi.nlm.nih.gov/20890285/
86. Kobayashi Y, Bustos MA, Hayashi Y, Yu Q, Hoon D. Interferon-induced factor 16 is essential in metastatic melanoma to maintain STING levels and the immune responses upon IFN-γ response pathway activation. J Immunother Cancer. 2024;12. Available from: https://pubmed.ncbi.nlm.nih.gov/39424359/
87. Fu XQ, Liu B, Wang YP, Li JK, Zhu PL, Li T et al. Activation of STAT3 is a key event in TLR4 signaling-mediated melanoma progression. Cell Death Dis. 2020;11. Available from: https://pubmed.ncbi.nlm.nih.gov/32312954/
88. Gassenmaier M, Rentschler M, Fehrenbacher B, Eigentler TK, Ikenberg K, Kosnopfel C et al. Expression of DNA Methyltransferase 1 Is a Hallmark of Melanoma, Correlating with Proliferation and Response to B-Raf and Mitogen-Activated Protein Kinase Inhibition in Melanocytic Tumors. Am J Pathol. 2020;190:2155–64. Available from: https://pubmed.ncbi.nlm.nih.gov/32679231/
89. Chen G, Huang AC, Zhang W, Zhang G, Wu M, Xu W et al. Exosomal PD-L1 contributes to immunosuppression and is associated with anti-PD-1 response. Nature. 2018;560:382–6. Available from: https://pubmed.ncbi.nlm.nih.gov/30089911/
90. Massi D, Brusa D, Merelli B, Ciano M, Audrito V, Serra S et al. PD-L1 marks a subset of melanomas with a shorter overall survival and distinct genetic and morphological characteristics. Ann Oncol. 2014;25:2433–42. Available from: https://pubmed.ncbi.nlm.nih.gov/25223485/
91. Lv H, Lv G, Chen C, Zong Q, Jiang G, Ye D et al. NAD + Metabolism Maintains Inducible PD-L1 Expression to Drive Tumor Immune Evasion. Cell Metab. 2021;33:110–127.e5. Available from: https://pubmed.ncbi.nlm.nih.gov/33171124/
92. Chen KC, Dhar T, Chen CR, Chen ECY, Peng CC. Nicotinamide phosphoribosyltransferase modulates PD-L1 in bladder cancer and enhances immunotherapeutic sensitivity. Biochim Biophys Acta Mol Basis Dis. 2024;1870. Available from: https://pubmed.ncbi.nlm.nih.gov/38428685/
93. Carbone F, Liberale L, Bonaventura A, Vecchié A, Casula M, Cea M, et al. Regulation and function of extracellular nicotinamide phosphoribosyltransferase/visfatin. Compr Physiol. 2017;7:603–21.
94. Frumento G, Rotondo R, Tonetti M, Damonte G, Benatti U, Ferrara GB. Tryptophan-derived Catabolites Are Responsible for Inhibition of T and Natural Killer Cell Proliferation Induced by Indoleamine 2,3-Dioxygenase. Journal of Experimental Medicine. 2002;196:459–68. Available from: https://doi.org/10.1084/jem.20020121
95. Uyttenhove C, Pilotte L, Théate I, Stroobant V, Colau D, Parmentier N et al. Evidence for a tumoral immune resistance mechanism based on tryptophan degradation by indoleamine 2,3-dioxygenase. Nature Medicine 2003 9:10. 2003;9:1269–74. Available from: https://www.nature.com/articles/nm934
96. Rad Pour S, Morikawa H, Kiani NA, Yang M, Azimi A, Shafi G et al. Exhaustion of CD4 + T-cells mediated by the Kynurenine Pathway in Melanoma. Sci Rep. 2019;9. Available from: https://pubmed.ncbi.nlm.nih.gov/31434983/
97. Becker AL, Indra AK. Oxidative Stress in Melanoma: Beneficial Antioxidant and Pro-Oxidant Therapeutic Strategies. Cancers. 2023;15:3038. Available from: https://www.mdpi.com/2072-6694/15/11/3038/htm
98. Schadendorf D, Zuberbier T, Diehl S, Czarnetzki BM. Serum manganese superoxide dismutase is a new tumour marker for malignant melanoma. Melanoma Res. 1995;5:351–3. Available from: https://pubmed.ncbi.nlm.nih.gov/8541726/
99. Hoejberg L, Bastholt L, Johansen JS, Christensen IJ, Gehl J, Schmidt H. Serum interleukin-6 as a prognostic biomarker in patients with metastatic melanoma. Melanoma Res. 2012;22:287–93. Available from: https://pubmed.ncbi.nlm.nih.gov/22617301/
100. Fukuda M. Rab GTPases: Key players in melanosome biogenesis, transport, and transfer. Pigment Cell Melanoma Res. 2021;34:222–35. Available from: https://onlinelibrary.wiley.com/doi/full/https://doi.org/10.1111/pcmr.12931
101. Patwardhan A, Bardin S, Miserey-Lenkei S, Larue L, Goud B, Raposo G et al. Routing of the RAB6 secretory pathway towards the lysosome related organelle of melanocytes. Nat Commun. 2017;8. Available from: https://pubmed.ncbi.nlm.nih.gov/28607494/
102. Liu Y, Li X, Chen S, Zhu C, Shi Y, Dang S et al. Pan-cancer analysis of SERPINE family genes as biomarkers of cancer prognosis and response to therapy. Front Mol Biosci. 2023;10:1277508. Available from: https://xena.ucsc.edu/
103. Wu M, Sarkar C, Guo B. Regulation of Cancer Metastasis by PAK2. International Journal of Molecular Sciences. 2024, Vol 25, Page 13443. 2024;25:13443. Available from: https://www.mdpi.com/1422-0067/25/24/13443/htm
104. Ablain J, Al Mahi A, Rothschild H, Prasad M, Aires S, Yang S et al. Loss of NEC-TIN1 triggers melanoma dissemination upon local IGF1 depletion. Nat Genet. 2022;54:1839–52. Available from: https://pubmed.ncbi.nlm.nih.gov/36229674/
105. Paolillo M, Schinelli S. Extracellular Matrix Alterations in Metastatic Processes. International Journal of Molecular Sciences. 2019;20:4947. Available from: https://www.mdpi.com/1422-0067/20/19/4947/htm
106. Ahrens T, Sleeman JP, Schempp CM, Howells N, Hofmann M, Ponta H et al. Soluble CD44 inhibits melanoma tumor growth by blocking cell surface CD44 binding to hyaluronic acid. Oncogene. 2001;20:3399–408. Available from: https://pubmed.ncbi.nlm.nih.gov/11423990/
107. Ho P, Melms JC, Rogava M, Frangieh CJ, Poźniak J, Shah SB et al. The CD58-CD2 axis is co-regulated with PD-L1 via CMTM6 and shapes anti-tumor immunity. Cancer Cell. 2023;41:1207–1221.e12. Available from: https://pubmed.ncbi.nlm.nih.gov/37327789/
108. Miguel RN, Wong J, Westoll JF, Brooks HJ, O'Neill LAJ, Gay NJ et al. A dimer of the Toll-like receptor 4 cytoplasmic domain provides a specific scaffold for the recruitment of signalling adaptor proteins. PLoS One. 2007;2. Available from: https://pubmed.ncbi.nlm.nih.gov/17726518/
109. Gasparrini M, Mazzola F, Cuccioloni M, Sorci L, Audrito V, Zamporlini F et al. Molecular insights into the interaction between human nicotinamide phosphoribosyltransferase and Toll-like receptor 4. J Biol Chem. 2022;298. Available from: https://pubmed.ncbi.nlm.nih.gov/35120922/
110. Ubanako P, Xelwa N, Ntwasa M. LPS induces inflammatory chemokines via TLR-4 signalling and enhances the Warburg Effect in THP-1 cells. PLoS One. 2019;14. Available from: https://pubmed.ncbi.nlm.nih.gov/31560702/
111. Madden EC, Gorman AM, Logue SE, Samali A. Tumour cell secretome in chemoresistance and tumour recurrence. Trends Cancer. 2020;6:489–505.
112. Qu Y, Dou B, Tan H, Feng Y, Wang N, Wang D. Tumor microenvironment-driven non-cell-autonomous resistance to antineoplastic treatment. Mol Cancer. 2019;18. Available from: https://pubmed.ncbi.nlm.nih.gov/30927928/
113. Semeradtova A, Liegertova M, Herma R, Capkova M, Brignole C, Del Zotto G. Extracellular vesicles in cancer´s communication: messages we can read and how to answer. Mol Cancer. 2025;24. Available from: https://pubmed.ncbi.nlm.nih.gov/40108630/
114. Kluszczynska K, Czyz M. Extracellular Vesicles-Based Cell-Cell Communication in Melanoma: New Perspectives in Diagnostics and Therapy. Int J Mol Sci. 2023;24. Available from: https://pubmed.ncbi.nlm.nih.gov/36674479/
115. Hirosawa KM, Sato Y, Kasai RS, Yamaguchi E, Komura N, Ando H et al. Uptake of small extracellular vesicles by recipient cells is facilitated by paracrine adhesion signaling. Nature Communications 2025 16:1. 2025;16:1–24. Available from: https://www.nature.com/articles/s41467-025-57617-9
116. Németh K, Kestecher BM, Ghosal S, Bodnár BR, Kittel Á, Hambalkó S et al. Therapeutic and pharmacological applications of extracellular vesicles and lipoproteins. Br J Pharmacol. 2024;181:4733–49. Available from: https://onlinelibrary.wiley.com/doi/full/https://doi.org/10.1111/bph.17336
117. Peinado H, Alečković M, Lavotshkin S, Matei I, Costa-Silva B, Moreno-Bueno G et al. Melanoma exosomes educate bone marrow progenitor cells toward a pro-metastatic phenotype through MET. Nature Medicine 2012 18:6. 2012;18:883–91. Available from: https://www.nature.com/articles/nm.2753
118. Sheokand N, Kumar S, Malhotra H, Tillu V, Raje CI, Raje M. Secreted glyceraldehye-3-phosphate dehydrogenase is a multifunctional autocrine transferrin receptor for cellular iron acquisition. Biochim Biophys Acta.

2013;1830:3816–27. Available from: https://pubmed.ncbi.nlm.nih.gov/23541988/
119. Schofield L, Lincz LF, Skelding KA. Unlikely role of glycolytic enzyme α-enolase in cancer metastasis and its potential as a prognostic biomarker. J Cancer Metastasis Treat. 2020;6:10. Available from: https://www.oaepublish.com/articles/2394-4722.2019.43
120. Li Y, Zhang Y, Dorweiler B, Cui D, Wang T, Woo CW et al. Extracellular Nampt promotes macrophage survival via a nonenzymatic interleukin-6/STAT3 signaling mechanism. J Biol Chem. 2008;283:34833–43. Available from: https://pubmed.ncbi.nlm.nih.gov/18945671/
121. Nacarelli T, Lau L, Fukumoto T, Zundell J, Fatkhutdinov N, Wu S et al. NAD + metabolism governs the proinflammatory senescence-associated secretome. Nat Cell Biol. 2019;21:397–407. Available from: https://pubmed.ncbi.nlm.nih.gov/30778219/
122. Liu W, Zhu M, Li X, Er L, Li S. NNMT Is an Immune-Related Prognostic Biomarker That Modulates the Tumor Microenvironment in Pan-Cancer. Dis Markers. 2023. Available from: https://pubmed.ncbi.nlm.nih.gov/36817086/
123. Eckert MA, Coscia F, Chryplewicz A, Chang JW, Hernandez KM, Pan S et al. Proteomics reveals NNMT as a master metabolic regulator of cancer-associated fibroblasts. Nature. 2019;569:723–8. Available from: https://pubmed.ncbi.nlm.nih.gov/31043742/
124. Mak TK, Li K, Zhao Z, Wang K, Zeng L, He Q et al. m6A demethylation of NNMT in CAFs promotes gastric cancer progression by enhancing macrophage M2 polarization. Cancer Lett. 2024;611. Available from: https://pubmed.ncbi.nlm.nih.gov/39725153/
125. Torretta S, Colombo G, Travelli C, Boumya S, Lim D, Genazzani AA et al. The Cytokine Nicotinamide Phosphoribosyltransferase (eNAMPT; PBEF; Visfatin) Acts as a Natural Antagonist of C-C Chemokine Receptor Type 5 (CCR5). Cells. 2020;9. Available from: https://pubmed.ncbi.nlm.nih.gov/32098202/
126. Lee CH, Wu CL, Shiau AL. Toll-like receptor 4 signaling promotes tumor growth. J Immunother. 2010;33:73–82. Available from: https://pubmed.ncbi.nlm.nih.gov/19952954/
127. Bockwoldt M, Houry D, Niere M, Gossmann TI, Reinartz I, Schug A et al. Identification of evolutionary and kinetic drivers of NAD-dependent signaling. Proc Natl Acad Sci U S A. 2019;116:15957–66. Available from: https://pubmed.ncbi.nlm.nih.gov/31341085/

Publisher's note